J. Fluid Mech. (1989), *vol.* 202, *pp.* 403–442
Printed in Great Britain

A natural low-frequency oscillation of the flow over an airfoil near stalling conditions

By K. B. M. Q. ZAMAN,[1] D. J. McKINZIE[1] AND C. L. RUMSEY[2]

[1] NASA Lewis Research Center, Cleveland, OH 44135, USA

[2] NASA Langley Research Center, Hampton, VA 23665, USA

(Received 22 April 1988)

An unusually low-frequency oscillation in the flow over an airfoil is studied experimentally as well as computationally. Wind-tunnel measurements are carried out with two-dimensional airfoil models in the chord Reynolds number (R_c) range of 0.15×10^5–3.0×10^5. During deep stall, at $\alpha \gtrsim 18°$, the usual 'bluff-body shedding' occurs at a Strouhal number, $St_s \approx 0.2$. But at the onset of static stall around $\alpha = 15°$, a low-frequency periodic oscillation is observed, the corresponding St_s being an order of magnitude lower. The phenomenon apparently takes place only with a transitional state of the separating boundary layer. Thus, on the one hand, it is not readily observed with a smooth airfoil in a clean wind tunnel, while on the other, it is easily removed by appropriate 'acoustic tripping'. Details of the flow field for a typical case are compared with a case of bluff-body shedding. The flow field is different in many ways from the latter case and does not involve a Kármán vortex street. The origin of the flow fluctuations traces to the upper surface of the airfoil and is associated with a periodic switching between stalled and unstalled states. The mechanism of the frequency selection remains unresolved, but any connection to blower instabilities, acoustic standing waves or structural resonances has been ruled out.

A similar result has been encountered computationally using a two-dimensional Navier–Stokes code. While with the assumption of laminar flow, wake oscillation akin to the bluff-body shedding has been observed previously, the St_s is found to drop to about 0.03 when a 'turbulent' boundary layer is assumed. Details of the flow field and unsteady forces, computed for the same conditions as in the experiment, compare reasonably well with the experimental data.

The phenomenon produces intense flow fluctuations imparting much larger unsteady forces to the airfoil than that experienced in bluff-body shedding, and may represent the primary aerodynamics of stall flutter of blades and wings.

1. Introduction

The low-frequency oscillation of flow over an airfoil was observed at NASA Langley by Zaman, Bar-Sever & Mangalam (1987), based on wake velocity spectra measurements. The spectra exhibited a sharp spike at an unusually low frequency which varied continuously with the free-stream speed. The corresponding Strouhal number ($St_s = f_s c \sin\alpha / U_\infty$, where f_s is the shedding (or flow oscillation) frequency, c the airfoil chord, α the angle of incidence and U_∞ the free-stream mean velocity) was only about 0.02. This compares to order(s) of magnitude higher values observed previously in cases involving bluff-body shedding (Roshko 1954), trailing-edge noise (Brooks & Schlinker 1983), etc. In order to obtain a better understanding of the

phenomenon, the present experiments were carried out. In the initial attempt in the relatively clean wind tunnel at NASA Lewis, the phenomenon could not be reproduced, but it could be when the tunnel free-stream turbulence was raised artificially, or tripping was applied near the leading edge, or the flow was excited acoustically at some high frequencies. Preliminary results were reported by Zaman & McKinzie (1988). Parametric dependence, details of the flow field for a typical case, and the effect of acoustic excitation in enhancing as well as suppressing the phenomenon were then explored.

A literature search yielded a few earlier works reporting fluctuations in flows over airfoils at frequencies much lower than the 'Strouhal frequency' of $St_s \approx 0.2$. Note that the term 'low frequency' is used in this sense to denote St_s values much lower than 0.2. The latter value, of course, represents the approximate Strouhal number of vortex shedding in the wake of bluff bodies (see also Schlichting 1979; Motallebi & Norbury 1981; Cendenese, Cerri & Ianetta 1981). Most wake oscillations reported in the literature translate to this Strouhal number if appropriate cross-stream lengthscales are used. For example, the trailing-edge noise studied by Brooks & Schlinker (1983) also yields this number if the trailing-edge thickness (with boundary-layer correction) is used as the lengthscale. In fact, it is not an exaggeration to say that whenever a wake oscillation is encountered, a fluid dynamicist's first reaction is to look for the 'Strouhal frequency'. The oscillation frequency under the present study is considered low since there is no apparent lengthscale that will produce a Strouhal number of 0.2. Here, let us note that while various non-dimensional frequency parameters have been used in previous airfoil studies, e.g. in connection with stall flutter, dynamic stall, etc., wherever possible these will be converted to St_s to be consistent in the present discussion.

A few very early studies at Cambridge reported low-frequency force fluctuations on stalling airfoils. Jones (1933) observed 'violent fluctuations' of lift and drag occurring around the angle of maximum lift. The fluctuations were at very low frequencies, as he described, '...at 14 degrees incidence with the balance weights adjusted to lie between the upper and lower limits... the balance arm continually moved to and fro between the upper and the lower stops at intervals which, though not exactly constant, were of the order of half a second'. From the data given in the experimental procedures, this converts to an St_s of only 0.006. Through meticulous, systematic measurements with the experimental tools of the time, Jones (1933, 1934) described three different stalling processes associated with airfoils of different cross-sectional shapes. He noted, as further elaborated in the text, that the violent fluctuations took place along with two of these stall processes.

Farren (1935) subsequently used a 'fast response balance' primarily to study lift and drag forces on oscillating airfoils. But he also reported a set of data for a fixed airfoil (model R.A.F. 28×1.07, at $\alpha = 14°$, $R_c = 10^5$), in which the normal force varied quasi-periodically with a period that corresponded to 'about 13 chords travel of the wing'. This converts to $St_s = 0.019$!

There have been numerous subsequent experiments on two-dimensional airfoils, including in the low-Reynolds-number range covered by Farren and Jones – see e.g. the excellent reviews by Carmichael (1981) and Mueller (1985). But somewhat surprisingly, to the best of the authors' knowledge, the low-frequency unsteady fluctuations have neither been pursued nor observed any further. Why one could only speculate. First, the phenomenon seems to take place in 'dirtier' flows, possibly explaining why it was not readily observed in the 'cleaner' wind tunnels of later experiments. Secondly, it is sensitive to ambient conditions. Thus, even if observed

it might have been considered a 'parasitic problem', somehow avoided or gotten rid of, and the experimentalist moved on. Furthermore, very low-frequency energy in the spectra in similar situations is often ignored and not looked for in appropriate analysis bands.

However, several experiments reported data, while dealing with various aspects of airfoils and blades, that translate to a low-frequency flow or force fluctuation. Moss (1979) studied the acoustic excitation effect on unsteady stall on a 0.5 m chord airfoil for up to $R_c = 4 \times 10^5$. From normal force spectra, he reported large-amplitude fluctuations occurring naturally at $St_s = 0.05$ and lower; moreover, he could pace the unsteady stall by periodic bursts of a high-frequency tone and the resulting unsteady forces were largest in the above St_s range.

There have been observations of similar low frequencies in stall flutter of blades and wings. For example, the upper frequency limit of compressor blade flutter presented by Armstrong & Stevenson (1960) (assuming 15° incidence and the velocity at midradius to correspond to U_∞) converts to an St_s of 0.012 for 'flexural flutter' and 0.05 for 'torsional flutter'. Stall flutter will be discussed further in the text, but its possible connection to the low-frequency phenomenon has provided added motivation for the present study.

Low-frequency oscillations have also been observed in various other separating flows. These include transitory stall in diffusers, flow behind steps, etc. Simpson (1985) provides a review; see also, Rockwell (1983). However, a 'resonance-like' behaviour as observed in the present study has not been reported in any of these cases.

Recently, there has been a controversial observation of such a resonance-like fluctuation in the wake of a circular cylinder. Sreenivasan (1985) reported a velocity spectral peak at a frequency 'incommensurately' lower than the expected 'Strouhal frequency'. Peaks at both frequencies, together with several others at the sum and difference frequencies and their harmonics, appeared in the spectra. With increasing Reynolds number, a sequence of transformations took place from 'orderliness' to 'chaos' and the re-emergence of 'orderliness', within the Reynolds-number range of 35–170 covered in the experiment. Sreenivasan considered these sequences as a precursor to transition, from the perspective of a nonlinear dynamical system. However, Van Atta & Gharib (1987) in a subsequent investigation, traced the origin of the lower frequency flow fluctuations to cylinder vibration. They observed that, depending on the flow and the cylinder (wire) tension, the spectra contained peaks at the main Strouhal frequency and at a certain (super)harmonic of the fundamental vibration frequency, the difference between the two corresponding to the lower frequency peak. However, K. R. Sreenivasan (private communication), based on a repeated experiment, maintains that the cylinder vibration is not a necessary condition for the generation of the lower frequency components.

In any case, the question naturally arises as to whether the low-frequency oscillation in the airfoil wake can also be traced to structural vibrations. This has been addressed through simultaneous flow and vibration measurements. As will be discussed below, the data clearly indicate that the oscillations under study are independent of the structural vibration characteristics.

A further indication that the phenomenon has its origin in the fluid dynamics and not in the structural resonances came from a computational study initiated by Anderson, Thomas & Rumsey (1984) and continued by Rumsey (1987). Using a compressible, two-dimensional, Navier–Stokes code, Rumsey (1987) computed the flow over a NACA0012 airfoil, without any imposed perturbation, at $R_c = 10^6$ and

$M = 0.3$. A low-frequency oscillation in the flow was encountered, if a turbulent boundary layer from near the leading edge was assumed. If, instead, a laminar boundary layer was assumed, oscillation similar to bluff-body shedding resulted. In spite of the question of the applicability of turbulence models to unsteady, stalled flows, the turbulent flow computation was seen to produce flow-field details that were remarkably similar to those obtained experimentally. It was felt strongly that the essential features of the phenomenon were captured by the computation. At this point, a joint effort was undertaken for further investigation. The computation was performed for the same airfoil shape and Reynolds number as in the experiment. This yielded a low-frequency periodic oscillation at $St_s = 0.03$. Details of the flow field were then computed and are discussed *vis-à-vis* the experimental data.

As already indicated, various aspects of the phenomenon have remained unexplained. The objective of this paper is to present data describing its main features. This is well justified as, to our estimation, this curious phenomenon has not only gone practically unrecognized in the fifty years or so of airfoil research but may also provide a clearer understanding of the fluid dynamics of stall flutter. The main body of the discussion will be included with the experimental results in §3, preceded by a description of the experimental procedures in §2. The computational results and associated details will be discussed in §4, followed by the conclusions in §5.

2. Experimental facility

The experiments were carried out in a low-speed wind tunnel having a test section with 76 × 51 cm cross-section (figure 1*a*). The flow entered through a 16 : 1 contraction section with five screens, passed through the test section and was then exhausted by an axial fan. The free-stream turbulence intensity was less than 0.1 %, but could be increased by installing turbulence-generating screens 37 cm upstream from the airfoil support. The two-dimensional airfoil model, used for most of the data, was of the same cross-sectional shape as in the Langley experiment (LRN(1)-1007, to be simply referred to as LRN). *Unless otherwise stated, the data reported are for this airfoil with $c = 12.7$ cm and span equal to the tunnel width.* Results from a 7.3 cm and a 25.4 cm chord LRN airfoil, an NACA0012 ($c = 10.2$ cm) airfoil, a Wortmann FX 63-137 ($c = 12.7$ cm) airfoil, and a shorter 30 cm span LRN airfoil ($c = 12.7$ cm) will also be discussed.

The airfoil was supported rigidly, at the two ends, with respect to both torsion and lateral movements. Two 0.635 cm diameter rods, firmly connected to the ends, formed the support axis. These two rods passed through two cylindrical bearings housed in the tunnel walls. The bearings prevented any lateral motion; clamps outside the tunnel prevented any rotation about the axis. Most of the data were obtained in this support configuration. For lift and drag measurements, the support bearings had to be changed. In this case, the airfoil was supported on a spherical bearing on one end. Through a universal coupling the support rod on this end was connected to an automated angular positioning device. The support rod on the other end of the airfoil was suspended on the preloaded springs of the lift and drag load cells.

There was provision for acoustic excitation through an acoustic driver mounted on the ceiling of the test section. The sound entered through a 2.54 cm hole in the ceiling directly above the airfoil support axis. A 0.635 cm B & K microphone, flush mounted on the ceiling, monitored the sound pressure level. Velocity measurements

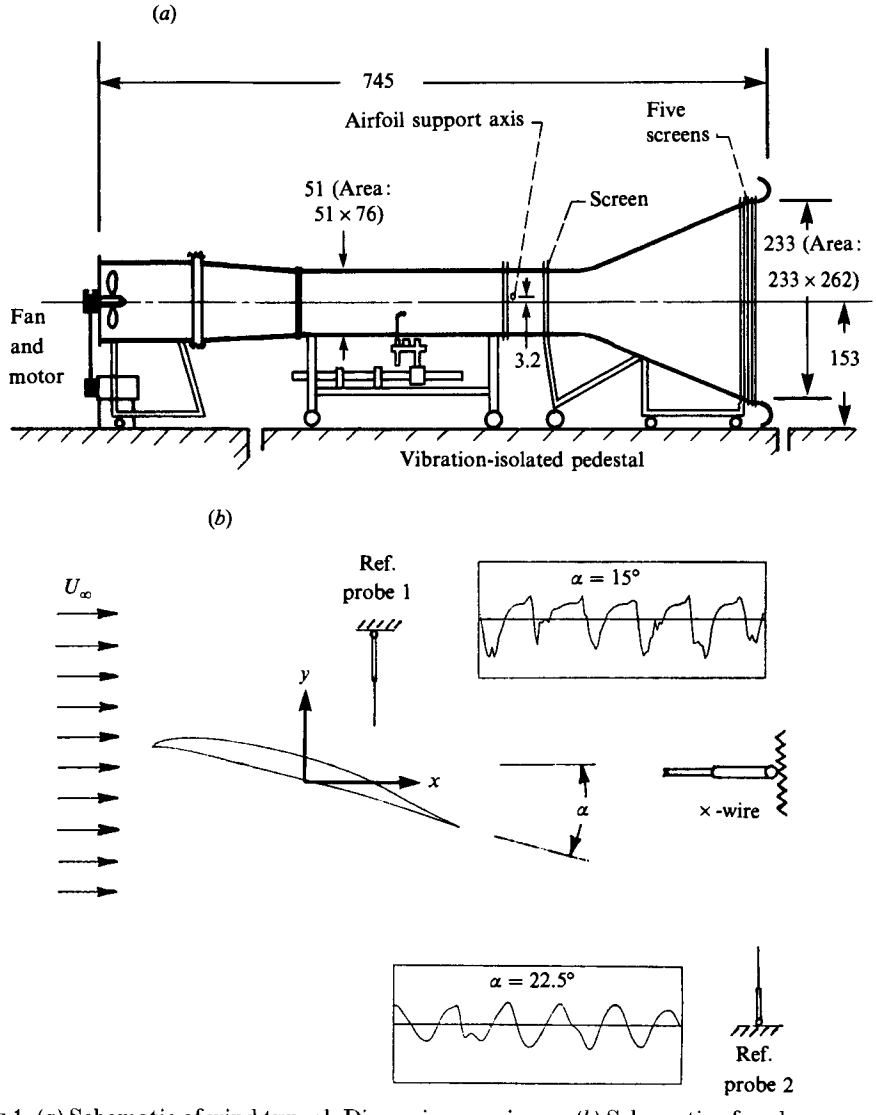

FIGURE 1. (*a*) Schematic of wind tunnel. Dimensions are in cm. (*b*) Schematic of probe arrangement. Insets are filtered u-signals from the reference probes at indicated angles of attack (α), at $R_c = 10^5$; record lengths are 732 ms and 112 ms for probes 1 and 2, respectively.

were made by standard hot-wire anemometry. Both single and crossed hot wires were used.

A schematic of the probe arrangement, used for conditional sampling measurements, to be elaborated on later, is shown in figure 1(*b*). The ×-wire probe could be traversed in the streamwise direction (x) through a longitudinal slot on the floor of the test section. For a given x, the entire slot was sealed; in this position, the probe could be moved up and down (in y) through automated computer (HP 9836) control without disturbing the seal. Unless otherwise stated, the airfoil is supported at midchord. The coordinate (x, y) origin is at the support axis, $z = 0$ is at the midspan of the test section.

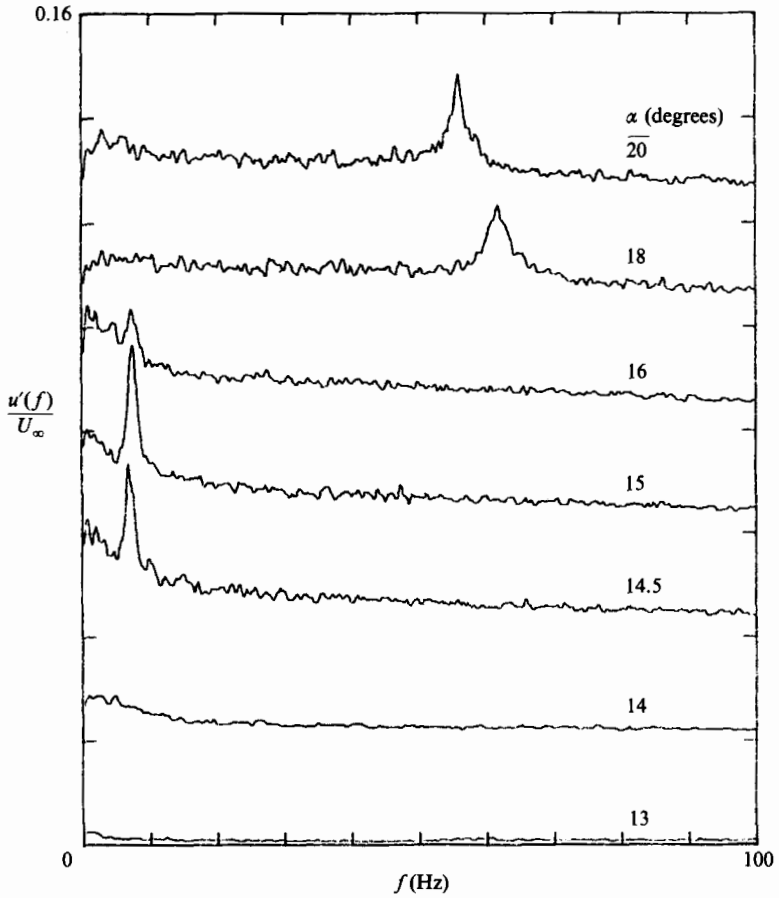

FIGURE 2. u'-spectra measured at $x/c = 1.5$, $z = 0$ and $y/c = 0.15$. Spectra traces are staggered successively by one ordinate division and are for indicated α. $R_c = 10^5$, $u'_\infty/U_\infty = 0.4\,\%$.

3. Experimental results

Figure 2 shows u'-spectra measured with a fixed hot wire about one chord downstream of the airfoil trailing edge. The free-stream turbulence was raised (with the screen placed upstream) to about 0.4 %. The spectra traces are for different α as indicated. At $\alpha = 18°$ and 20°, the spectral peaks at the relatively higher frequencies represent the bluff-body shedding and correspond to $St_s \approx 0.2$. Around $\alpha = 15°$, a spectral peak at 7.5 Hz occurs unambiguously. This corresponds to $St_s \approx 0.02$, a value found to remain approximately constant at other speeds and to agree with the previous data of Zaman *et al.* (1987). At lower α, the flow is attached and no spectral peaks occur in the frequency range covered. However, at certain lower α there were higher frequency peaks scaling on the airfoil thickness, i.e. yielding a Strouhal number of about 0.2, with the latter as the lengthscale. There is no cross-stream lengthscale apparent for the $\alpha = 15°$ case, however, that would produce the Strouhal number of 0.2. This is why the frequency in this case is considered unusually low.

As indicated earlier, the occurrence of the low-frequency oscillation had been illusive and puzzling. It could not be reproduced in the initial attempt. This can be appreciated from figure 3. With the normal tunnel operation, spectra traces similar

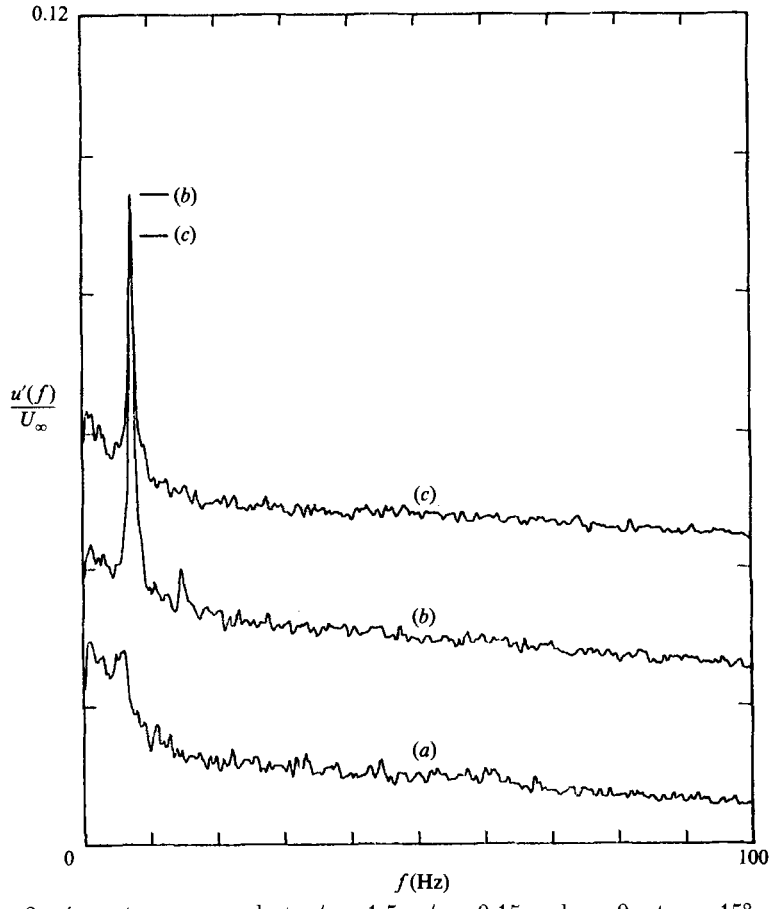

FIGURE 3. u'-spectra measured at $x/c = 1.5$, $y/c = 0.15$ and $z = 0$, at $\alpha = 15°$ and $R_c = 10^5$. (*a*) $u'_\infty/U_\infty = 0.1\%$; (*b*) $u'_\infty/U_\infty = 0.1\%$ with acoustic excitation at 2540 Hz; (*c*) $u'_\infty/U_\infty = 0.4\%$.

to (*a*) were obtained at first in which the sharp peak was absent. Only when the free-stream turbulence was increased did it result in the spectral spike as in trace (*c*). Trace (*b*) shows that a high-frequency acoustic excitation of a flow otherwise the same as in (*a*), also produced the low-frequency oscillation. (However, the acoustic excitation at even higher frequencies had the opposite effect of eliminating the low-frequency peak otherwise occurring naturally in case (*c*), see §3.3.) It was found later that adding an appropriate boundary-layer trip also produced the spectral spike as in (*b*) or (*c*) in a flow otherwise the same as in (*a*). (The trip was a strip of masking tape attached to the underside of the airfoil near the stagnation line. The tripping edge was about 2 mm downstream of the leading edge, protruded about 0.5 mm away from the surface, and had V-notches spaced about 0.5 cm in the spanwise direction. Tripping at various locations on the upper surface was found to be ineffective.)

Unless otherwise stated, the data shown are for smooth airfoils. The flow-field details were obtained at $R_c = 0.75 \times 10^5$. The flow visualization was easier at the lower R_c; the airfoil vibrations were also of smaller amplitudes, permitting hot-wire probing of the boundary layer.

3.1. *Role of structural vibration*

As mentioned before, the low-frequency flow oscillation imparted large unsteady forces to the airfoil. In fact, the airfoil started 'fluttering' as soon as it was loosened from its rigid mount, with increasing amplitude at higher R_c. Even when the airfoil was held rigidly, the midsection vibrated visibly, with a total displacement of about 1 mm at $R_c = 10^5$. On close inspection, the vibration was determined to be at the same low frequency as that of the flow, at all R_c.

As discussed in §1, there was concern that structural resonance may have played a role in inducing the flow oscillation. Note that it would be impossible to completely restrain the airfoil but the following indicates strongly that the vibration was a result of the unsteady flow and not vice versa: (1) The frequency varied continuously with U_∞, yielding a constant St_s in two different wind tunnels (the present and that of Zaman *et al.* 1987). (2) The oscillation appeared or disappeared in a flow and structural environment that was otherwise the same, depending only on the free-stream turbulence or a high-frequency acoustic excitation.

The role of structural vibration was probed by simultaneous hot-wire and accelerometer measurements. Two accelerometers were attached to the airfoil upper surface, with a hot-wire located downstream, as shown in the inset of figure 4(*a*). At $\alpha = 15°$ and $R_c = 0.75 \times 10^5$, the spectra of both acceleration signals (S_1 and S_2) exhibited peaks at about 36 Hz (figure 4*a*). The flow was undergoing the low-frequency oscillation at about 6 Hz, at which a small peak also appeared in S_1 and S_2. Note that the acceleration, being proportional to frequency squared, was of much larger amplitude at 36 Hz even though the corresponding displacement was smaller than that at 6 Hz. The middle trace, ϕ_{12}, represents the phase between the two acceleration signals (ordinate ranges $-180°$ to $180°$). At both 6 Hz and 36 Hz, the phase is zero indicating an in-phase motion. This excludes a (twisting) torsional vibration as the stimulant for the low-frequency flow oscillation. From visual stroboscopic observation, the vibration was found primarily at 6 Hz and was flexural (or bending) in nature.

With the flow turned off, light tapping on the airfoil support produced acceleration spectral peaks at about 36 Hz but nothing at around 6 Hz. An estimate, with the assumption that the airfoil is simply supported at the ends, produced a fundamental flexural resonance at 33 Hz. (The assumption should be reasonable since the two end rods are supported on the bearings and clamped outside the tunnel; the assumption of rigidly held ends, requiring zero slopes in bending, yields a resonance at the much higher frequency of 75 Hz.) The fundamental torsional resonance was roughly estimated to be also at a much higher frequency. Thus, the observed peak at 36 Hz must be due to the fundamental flexural resonance.

With the flow on, the simultaneously measured velocity spectrum, S_3, exhibits a peak only at 6 Hz. If there were bluff-body shedding at this α, the 'Strouhal frequency' would be expected at around 54 Hz. There are no peaks in S_3 at 36 Hz or 54 Hz. Thus, one cannot explain the low-frequency component in the way that Van Atta & Gharib (1987) did for the cylinder wake case. This is because their explanation was based on the fact that the low frequency equalled the difference between the Strouhal frequency and a harmonic of the cylinder vibration frequency, spectral peaks appearing at all three. Finally, the top trace in figure 4(*a*) shows the coherence between the signals from the hot wire and one of the accelerometers (ordinate ranges 0 to 1). While there is large coherence at 6 Hz and its immediate higher harmonics, there is none at the flexural resonance frequency. If the latter were

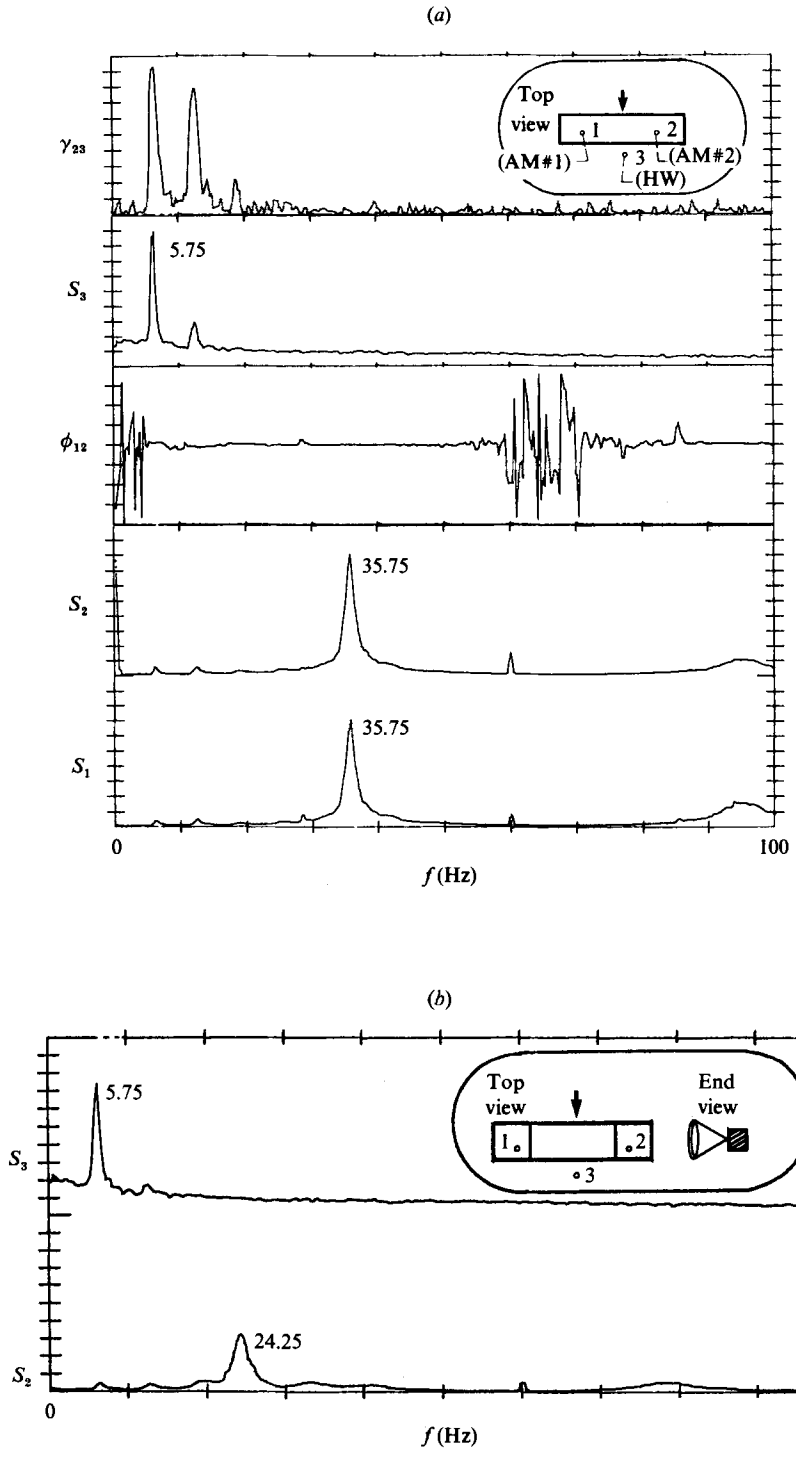

FIGURE 4. (*a*) Simultaneous accelerometer (AM) and hot-wire (HW) data. S denotes spectra, ϕ the phase, and γ the coherence; subscripts denote sensors as shown in the inset. $R_c = 0.75 \times 10^5$. (*b*) Measurements as in (*a*) with two 1 lb weights strung over the airfoil as shown in the inset.

pacing the flow oscillation, even though through some kind of coupling, one would expect significant coherence.

The structural resonance effect was probed further by intentionally loading the airfoils. Two 1 lb weights were strung over the airfoil as shown in the inset of figure 4(*b*). This changed the flexural resonance from 36 Hz to about 24 Hz. As can be observed from S_3, in spite of this the flow oscillation frequency remained unchanged. The data in figure 4(*a*, *b*) should be ample proof that the low-frequency flow oscillation under study is not a legacy of the structural resonance characteristics.

3.1.1. *Blower instability*

Forced flow fluctuations by blower rotational speed or blade passage was ruled out. For example, for the flow conditions of figure 4, the blower rotational speed was about 27 Hz – thus this and the blade passage frequency (162 Hz) were much higher than the flow oscillation at 6 Hz. An unstable blower operation, e.g. at certain ranges of the flow rate *vs.* pressure drop curve, was also ruled out. This was done by variably opening a window on the downstream end of the test section. The same U_∞ was realized with different blower r.p.m. for different widths of opening of the window. In spite of the change in the blower operation point, the flow oscillation frequency at $\alpha = 15°$ remained constant as long as U_∞ was held constant.

3.1.2. *Tunnel resonance*

The tunnel resonances were also at frequencies much higher than the flow frequency being considered. The tunnel resonant frequencies were determined by measuring sound pressure level L_R, and u' and v' at a certain reference location, while imparting acoustic excitation (Zaman & McKinzie 1989). The lowest was at 23 Hz corresponding to half-wave resonance in the entire length of the tunnel. There was longitudinal half-wave resonance at 59 Hz due to the length of the test section, and fundamental cross-resonances at 224 Hz and 345 Hz corresponding to the span and the height of the test section. The presence of the airfoil could set up resonances similar to those observed by Parker (1966). Even though this was not investigated thoroughly, the 'Parker modes' can also be expected at much higher frequencies near and above 345 Hz.

3.2. *The flow-field details*

Data on the unsteady flow field for a typical case of the low-frequency oscillation were acquired. In doing this, corresponding data were also acquired for a case of bluff-body shedding. These two cases were at (1) $\alpha = 15°$, yielding an oscillation at 5.75 Hz and (2) $\alpha = 22.5°$, yielding an oscillation at 35.5 Hz; both were at $R_c = 0.75 \times 10^5$, with a free-stream turbulence of 0.4 % (with the screen), but without any acoustic excitation. The two frequencies varied slightly from day to day and are nominally referred to as 6 Hz and 36 Hz, respectively.

Figure 5(*a*) shows the fundamental r.m.s. velocity fluctuation amplitudes, at the respective frequencies for the two cases, as a function of the streamwise distance. These measurements were made along the midspan at a constant height slightly above the airfoil upper surface. It is clear that the low-frequency oscillation has very large amplitude, but decays rapidly with x, the largest occurring at about $0.25c$ from the leading edge. For the bluff-body-shedding case, the amplitude is negligible over the airfoil and increases farther downstream.

Figure 5(*b*) shows the axial variation of the phase corresponding to the data of figure 5(*a*). The slopes, measured in the range $x/c > 2$, yielded wavelengths of about $8.5c$ and $1.8c$ for the low- and high-frequency cases, respectively; the

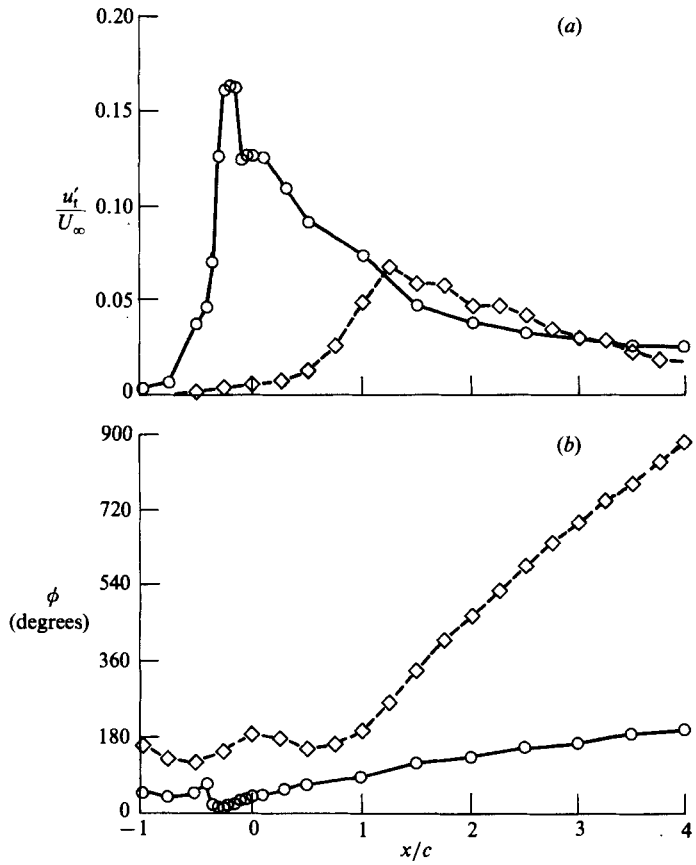

FIGURE 5. (*a*) u'_t/U_∞ *vs.* x/c at $y/c = 0.15$ and $z = 0$. $R_c = 0.75 \times 10^5$; $u'_\infty/U_\infty = 0.4\,\%$. Solid curve, $\alpha = 15°$; dashed curve, $\alpha = 22.5°$. (*b*) Corresponding phase variations.

corresponding phase velocities turned out to be about $0.7U_\infty$ and $0.95U_\infty$, respectively. The phase velocity result is further proof that the low-frequency oscillation is hydrodynamic in nature and not due to, say, a standing acoustic wave (§3.1.2).

The transverse variation of the fundamental amplitude and phase, one chord downstream from the trailing edge at midspan, are shown in figures 6(*a*) and 6(*b*). The amplitude for the low-frequency case, which was very large over the airfoil, has become comparable with that due to the bluff-body shedding. The latter is large across the wake indicating a larger kinetic energy flux due to the fluctuations at this x-station. The amplitude and phase data for the bluff-body-shedding case are indicative of a Kármán vortex street, which is confirmed later by conditionally averaged vorticity data.

The corresponding data for the $\alpha = 15°$ case only, measured over and below the airfoil at $x/c = -0.1$, are shown in figure 7. The data from figure 6 are repeated for easy comparison. The gaps in the curves represent regions that could not be accessed by the hot-wire mounted on a horizontal support. The amplitude is intense over the airfoil. The peak occurs about 8 mm from the surface where the local mean velocity is about 90 % of U_∞. Under the airfoil, the amplitude is small, clearly indicating that the origin of the low-frequency oscillation is on the upper surface.

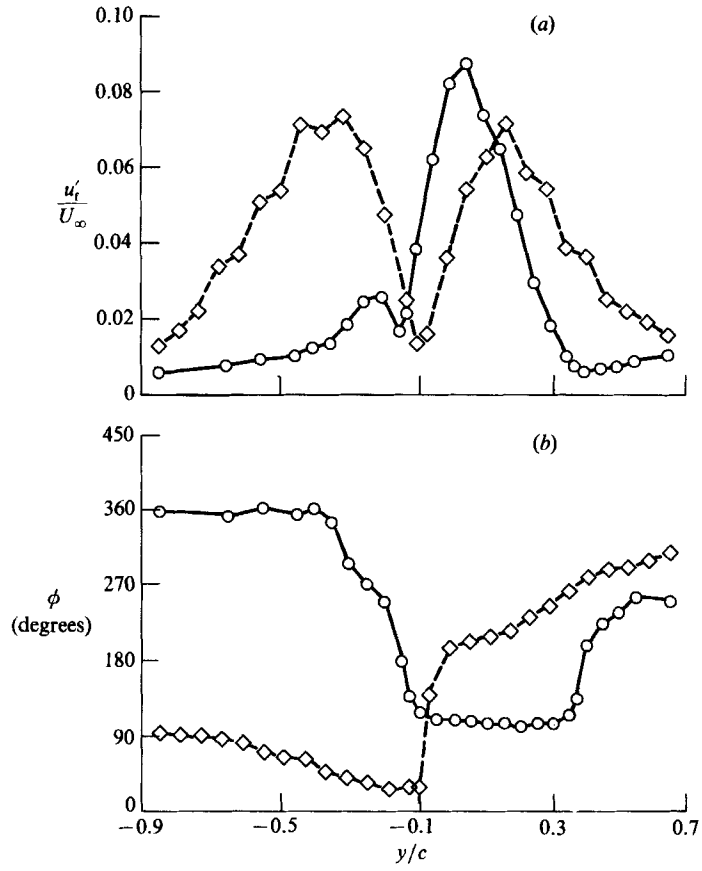

FIGURE 6. (*a*) u_f'/U_∞ *vs.* y/c at $z = 0$ and $x/c = 1.5$ for the two α-values of figure 5. (*b*) Corresponding phase variations.

The transverse phase variations for the $\alpha = 15°$ case at different x/c are shown in figure 8. The five lower curves represent measurements on the airfoil upper surface, the left end of each curve terminating on the surface. Note the gradual, consistent evolution of the $\phi(y)$ profile compared to that shown in figure 6(*b*). The validity of the approximately 90° phase jump near the airfoil surface, at $x/c = 0.1$ and 0.3, could be questioned because hot-wire rectification is expected due to flow reversal during part of the oscillation cycle. However, no flow reversal and hot-wire rectification are expected at $x/c = 1$ and downstream. Thus, the consistent evolution of the $\phi(y)$ profiles indicates that the phase has been measured correctly at all x-stations. Considering the plateaux around $y/c = 0.1$ or the higher levels to the right of each profile, the streamwise phase speed is found to remain approximately constant at all x. A motivation for obtaining this data set was to detect possible upstream-propagating waves through the boundary-layer region, to complete a feedback loop for sustaining the low-frequency oscillation. The data do not reveal the presence of any such wave within the measurement resolution and accuracy.

The boundary-layer profiles of U, the total r.m.s. (longitudinal) velocity fluctuation u_t', and the fundamental r.m.s. velocity fluctuation (at frequency f_s) u_f', as measured with a (single) hot wire, are shown in figures 9 and 10 for the $\alpha = 15°$ and $\alpha = 22.5°$ cases, respectively. The u_f' profile in figure 9 is a duplication of the data in figure 7,

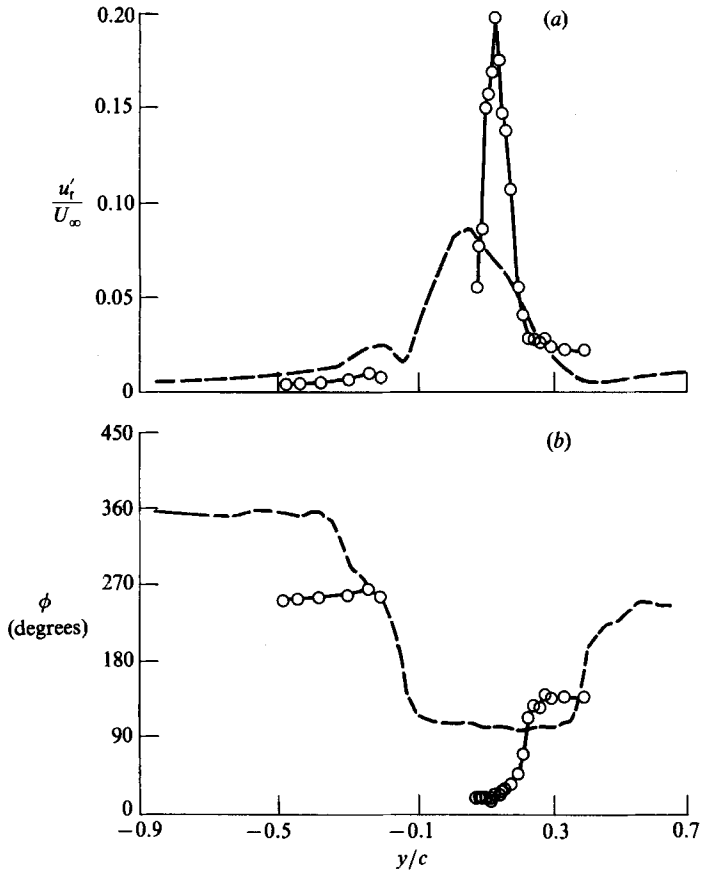

FIGURE 7. (*a*) u_t'/U_∞ *vs.* y/c for $\alpha = 15°$. Solid line, measurement at $x/c = -0.1$; dashed line, $x/c = 1.5$. (*b*) Corresponding phase variations.

and is shown for easy comparison with the u_t' data. Note that in both cases the mean velocity just outside the boundary layer is higher than U_∞. With increasing y, U drops and eventually should equal U_∞. Near the surface, there is separated flow at least during part of the oscillation cycle. There, flow reversal during those instants makes the measurements erroneous owing to hot-wire rectification. As a rough guideline, the amplitudes in figures 9 and 10 should be considered erroneous in regions where $U/U_\infty \lesssim 0.5$. Nevertheless, the measured profiles have been shown in their entirety as they provide an indication of the size of the recirculating zone. For the $\alpha = 22.5°$ case, the existence of a recirculating zone about 2 cm high is clearly apparent. In figure 9 u_f' is found to be comparable with u_t'; thus, the fluctuating flow field is dominated by the low-frequency oscillation. However, the latter is not strictly periodic, and dispersions as well as occasional dropouts account for the difference between u_t' and u_f'. In contrast, u_f' is negligible compared to u_t' in figure 10; the spectral peak at f_s was barely visible above the background turbulence in this case.

The spanwise variation of the amplitude and phase, similar to the data of figures 5 and 6, are shown in figure 11. These data have been obtained about one chord downstream of the trailing edge. At this x-station, the oscillations are hardly two-dimensional. Clearly, the disturbances originating from the junctions of the

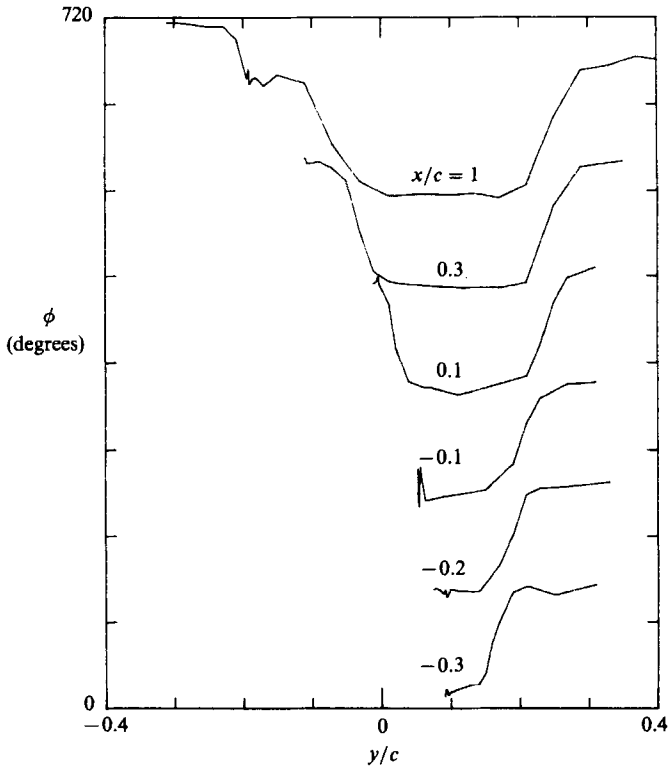

FIGURE 8. Transverse phase variations for $\alpha = 15°$ at indicated x-locations. Curves are staggered by 90°.

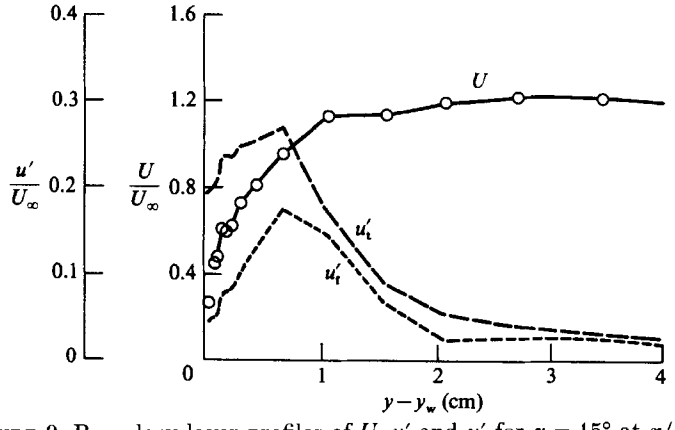

FIGURE 9. Boundary-layer profiles of U, u'_t and u'_l for $\alpha = 15°$ at $x/c = -0.1$. y_w is airfoil upper-surface location.

airfoil and the tunnel walls have influenced these variations. However, the flow over the airfoil, for either case, appeared from flow visualization experiments to be uniform along the span.

3.2.1. *Flow visualization*

Smoke-wire flow visualization movies were obtained. Specially fabricated 'knotted' wires (0.12 mm diameter wire, knots spaced about every 0.5 cm), were used. This provided relatively long smoke duration (of the order of 2 s), which was necessary

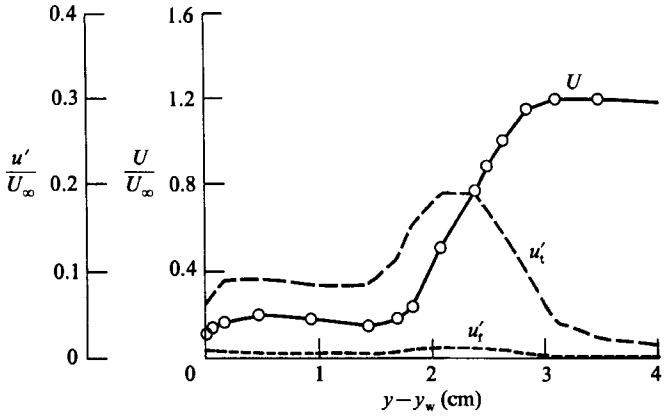

FIGURE 10. Profiles for $\alpha = 22.5°$, as in figure 9.

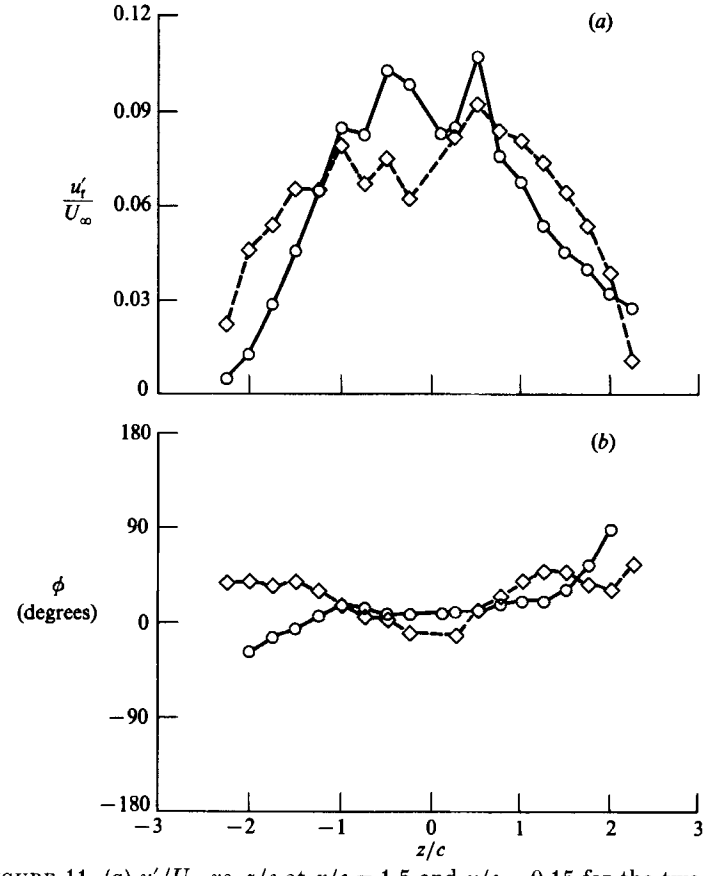

FIGURE 11. (*a*) u_t'/U_∞ *vs.* z/c at $x/c = 1.5$ and $y/c = 0.15$ for the two cases of figure 5. (*b*) Corresponding phase variations.

because of the low frequency involved in the $\alpha = 15°$ case. Unfortunately, this produced non-laminar smoke streaks resulting in poorer picture quality. The movies, however, showed the overall flow fields quite adequately.

The pictures in figure 12 were obtained with a horizontal smoke wire, placed about 4 cm upstream of the leading edge. Pairs of pictures, from the movie sequences,

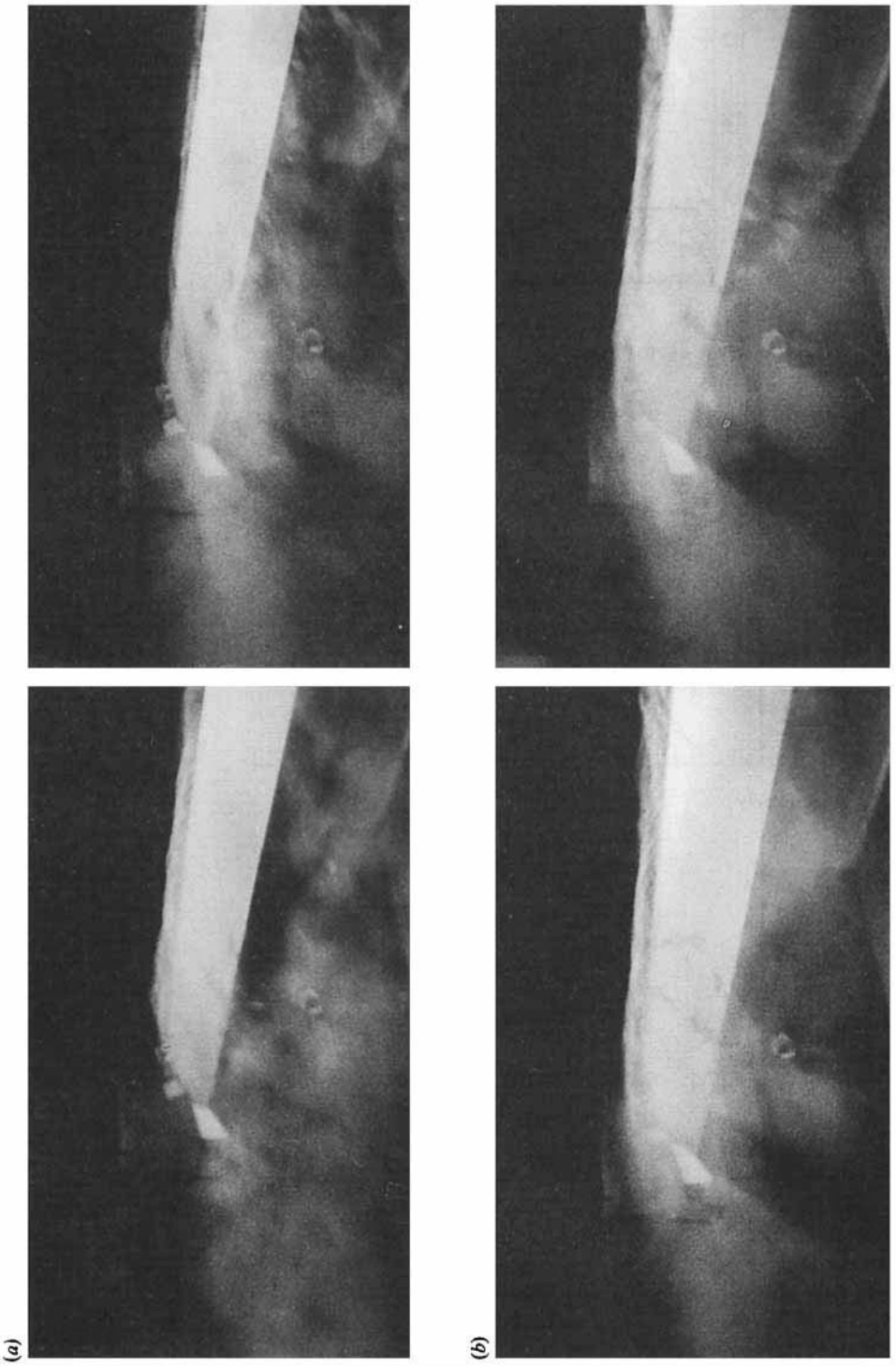

FIGURE 12. Flow visualization pictures (from movie sequence) using horizontal smoke wire. (*a*) $\alpha = 15°$, (*b*) $\alpha = 22.5°$.

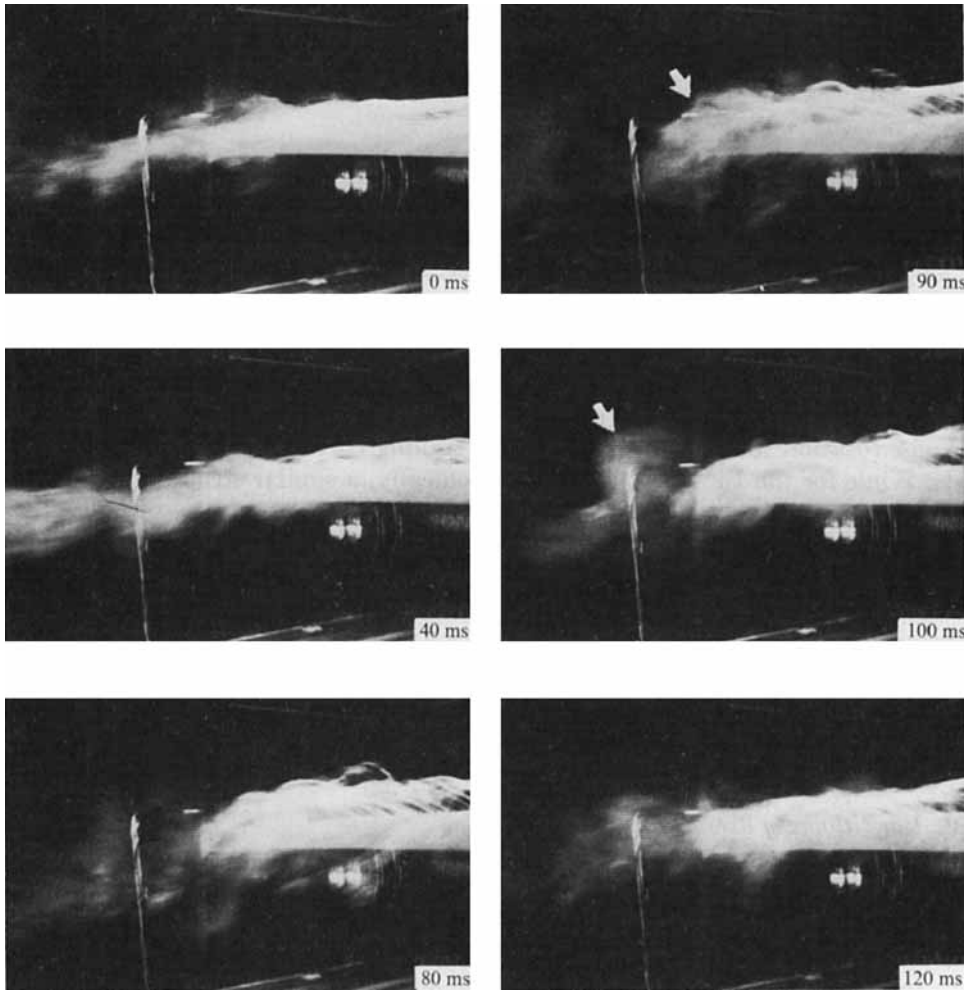

FIGURE 13. Flow visualization pictures for the flow of figure 12(*a*) from a different camera angle.

separated approximately 180° out of phase are shown. The silhouette of the leading edge behind the rising smoke streaks can be observed in each picture. In (*a*) for the $\alpha = 15°$ case, the right-hand picture exhibits a relatively more attached flow than that on the left-hand side. A periodic up and down 'flapping' motion of the smoke streaks was the most readily and easily discernible characteristic for this case. In comparison, the smoke streaks in (*b*) for the 22.5° case did not exhibit any such oscillation. The smoke streak patterns can be observed to be two-dimensional, i.e. uniform in the spanwise direction except near the tunnel walls. However, the flow field downstream rapidly developed three-dimensionality as indicated by figure 11 as well as flow visualization pictures shown in figure 13.

Figure 13 shows another set of pictures for the $\alpha = 15°$ case. The time differences, relative to the instant of the top picture, are indicated; note that the times are not equally spaced. The gradual buildup and the subsequent collapse of the separated region can be easily observed. A rapid development of three-dimensionality shortly downstream of the trailing edge can also be observed. A junction-vortex-like

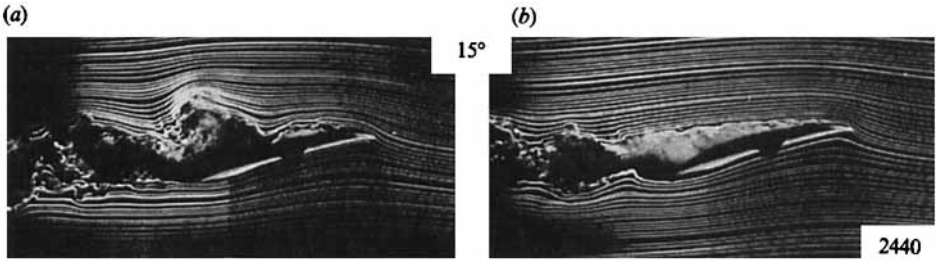

FIGURE 14. Flow visualization pictures using vertical smoke wire, reproduced from Zaman *et al.* (1987). $c = 10.2$ cm, $R_c = 0.40 \times 10^5$, $\alpha = 15°$, $f_s = 4.5$ Hz. (*a*) No excitation; (*b*) $f_p = 2440$ Hz.

structure appears in the pictures for 90 and 100 ms (marked by arrows), apparently forming shortly after the separation is maximum. Viewed from downstream, it has a clockwise rotation, and appears similar to a 'trailing vortex' (see e.g. Van Dyke 1982, p. 51). While for the 15° case it formed periodically, a similar structure appeared to be present continuously in the 22.5° case.

Flow visualization (still) photographs, using a vertical smoke wire, had been obtained for $\alpha = 15°$ in the earlier Langley experiment (Zaman *et al.* 1987). A pair of pictures, with and without acoustic excitation, are reproduced in figure 14. These pictures, for a lower U_∞ (6.1 ms^{-1}, $c = 10.2$ cm) taken with a straight smoke wire, show a much crisper view of the flow field. The flow without any excitation, on the left, was undergoing a low-frequency oscillation at 4.5 Hz. Upon acoustic excitation at a high frequency (2440 Hz) this oscillation was eliminated, the flow field for which is shown on the right. The excitation effect will be discussed further in §3.3.

3.2.2. *Conditionally averaged vorticity field*

Conditionally averaged spanwise vorticity data were acquired for the two cases under consideration. First, the nature of the two basic wakes on a time-average basis are further documented in figure 15(*a–c*). The U, u'_t, and total r.m.s. transverse velocity fluctuation v'_t profiles at $x/c = 1.5$ are shown. The wider and deeper wake for the $\alpha = 22.5°$ case (figure 15 *a*) represents a higher drag, as expected. The turbulence intensities are also higher for the 22.5° case.

The conditional averaging measurements were carried out with the help of an $\times$-wire and reference probes as shown in figure 1(*b*). The procedures are briefly described here. Filtered reference signals for the low-frequency case (probe 1) and the high-frequency case (probe 2), for $R_c = 10^5$, are shown in figure 1(*b*). For each y-location of the $\times$-wire probe, the u-, v- and the appropriate reference signals were recorded digitally. The negative peaks in the reference signals, discriminated by a threshold of 1.5σ, were used as triggers for data sampling; σ is the standard deviation of the respective reference signal. Centred around the triggers, records of u- and the v-signals were ensemble averaged assuming a triple decomposition,

$$\tilde{f} = F + f_c + f_r,$$

yielding,

$$\langle \tilde{f} \rangle = F + \langle f_c \rangle = \langle f \rangle.$$

F, f_c and f_r are the time-average, the 'coherent' and the 'incoherent' components of the instantaneous function $\tilde{f}$, respectively. The angle bracket denotes ensemble averaging, and the notation $\langle f \rangle$ is used to include the time-average F in the ensemble average.

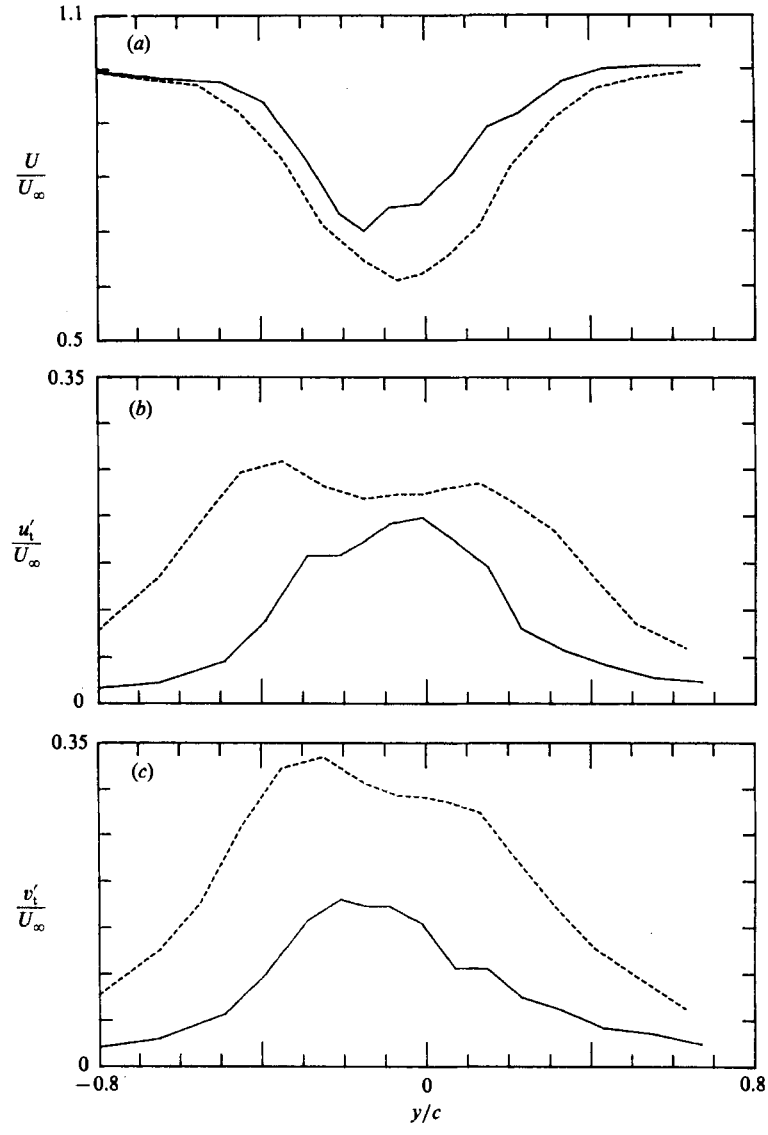

FIGURE 15. U, u_t' and v_t' profiles at $x/c = 1.5$ and $z = 0$. Solid line, $\alpha = 15°$; dashed line, $\alpha = 22.5°$.

The distributions of $\langle u \rangle$ and $\langle v \rangle$ as a function of time (τ) were obtained at different y. From these the ensemble-averaged spanwise vorticity was obtained by invoking the Taylor hypothesis (Zaman & Hussain 1981*b*):

$$\langle \Omega_z \rangle = \frac{-1}{0.7\, U_\infty} \frac{\partial \langle v \rangle}{\partial \tau} - \frac{\partial \langle u \rangle}{\partial y}.$$

$\langle \Omega_z \rangle$ has been non-dimensionalized by the constant c/U_∞ for both cases, the time axis having been normalized by the respective periods. Note that $\langle \Omega_z \rangle$ includes the time-average contribution, and that the convection velocity used in the Taylor hypothesis is $0.7\, U_\infty$. Figure 5(*b*) showed that the convection velocity for the $\alpha = 22.5°$ case was about $0.95 U_\infty$ for $x/c \gtrsim 2$ but lower farther upstream. It was

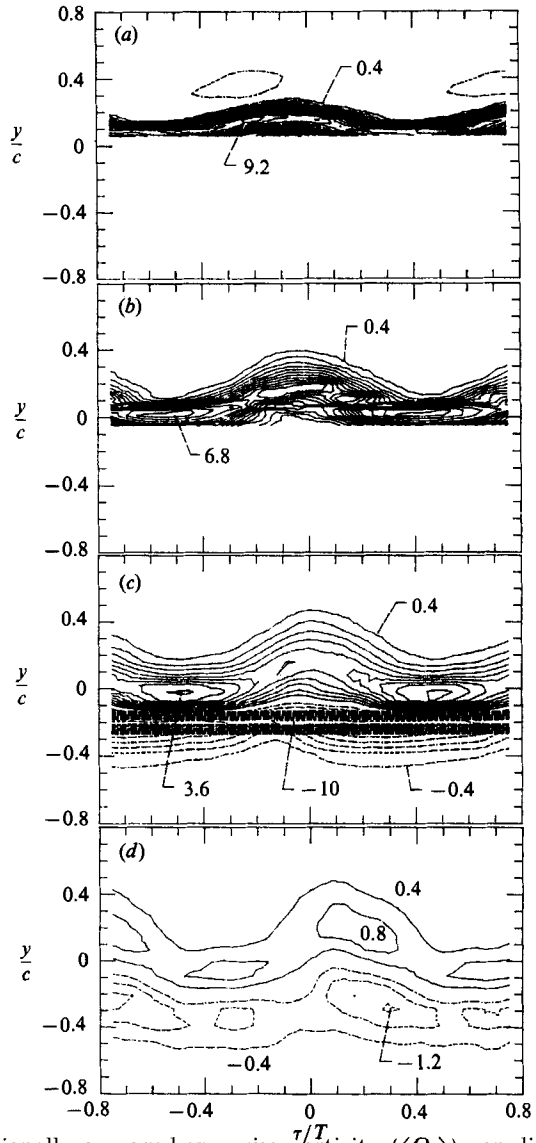

FIGURE 16. Conditionally averaged spanwise vorticity ($\langle \Omega_z \rangle$) non-dimensionalized by c/U_∞, for $\alpha = 15°$. The abscissae are normalized by the period (180 ms). Contour levels are in the sequence $\pm$(0.4, 0.8, 1.2..., 4.4, 5.2...). The measurement stations (x/c) are: (*a*) −0.1, (*b*) 0.2, (*c*) 0.5, (*d*) 1.5. Reference probe located as shown in figure 1(*b*).

found that the overall patterns of the $\langle \Omega_z \rangle$ contours did not change significantly if a convection velocity of $0.95U_\infty$ was used instead. The levels were affected somewhat; for example, the peak levels 2.55 and −3.89 in figure 17(*d*) (discussed shortly) changed to 2.13 and −3.34, respectively; this represents a departure of about 20% in the levels. For simplicity, the value $0.7U_\infty$ has been used throughout.

Data for the $\alpha = 15°$ case at indicated x-locations are shown in figure 16. A sheet of positive vorticity (clockwise), undulating with time, is observed on the upper surface. No 'roll-up' is observed in these temporal distributions. In figure 16(*c*), a sharp transverse drop in U right behind the trailing edge accounts for the large

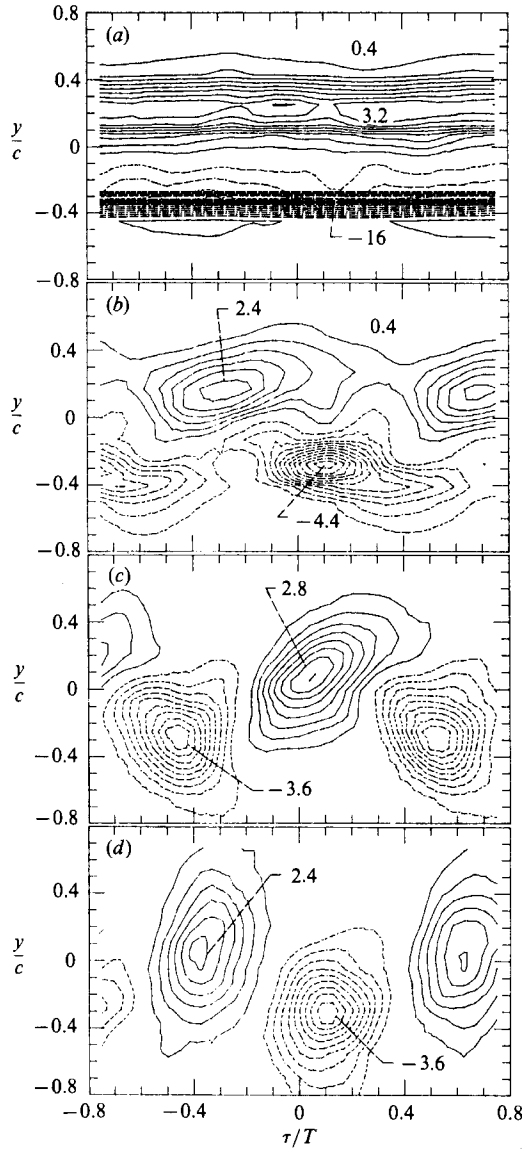

FIGURE 17. $\langle \Omega_z \rangle$ (c/U_∞) distributions as in figure 16 but for $\alpha = 22.5°$. Abscissae are normalized by the period 28 ms. The measurement stations (x/c) are: (*a*) 0.5, (*b*) 1.0, (*c*) 1.5 and (*d*) 2.5. Reference probe located as shown in figure 1(*b*).

negative $\langle \Omega_z \rangle$ levels appearing as a dark band in the contours. One finds that the high levels of $\langle \Omega_z \rangle$ diminish rapidly, and the distribution at $x/c = 1.5$ is not much different from that expected from the corresponding profile of $U(y)$ (figure 15*a*). Here, let us note that the flow field on the upper surface in the $\alpha = 15°$ case goes through a fast evolution (for further details see §4). The fast evolution throws doubt on the applicability of the Taylor hypothesis to the vorticity measurements. The spatial resolution with the × -wire is also poor in the separating shear layer over the upper surface. Thus, the distributions in figure 16(*a–c*) should be considered as qualitative.

The spatial resolution error is negligible for the rest of the vorticity data in figures 16–19, representing $x/c \geqslant 1$. For these data, application of the Taylor hypothesis is also reasonable (Zaman & Hussain 1981*b*), but probably constitutes the largest source of error in the vorticity amplitudes. Recall that using a different convection velocity in the hypothesis (for the data in figure 17*d*) results in a departure of 20% in the peak amplitudes. Contributions from other measurement errors, e.g. due to a large instantaneous flow angle relative to the $\times$-wire, should be relatively small. No further effort was made to assess the errors as that would require detailed analysis and additional experimentation.

Compared to the $\alpha = 15°$ case, significantly higher concentration of $\langle \Omega_z \rangle$ occurs in the 22.5° case even at $x/c = 2.5$, as shown in figure 17. Clearly, a Kármán-vortex-street-type structure evolves by the distance of $x/c = 1.5$. Note that just downstream of the trailing edge (in *a*), there is no undulation in the vorticity with time, the 'roll-up' commences farther downstream. The lack of fluctuation in the vorticity field in the vicinity of the airfoil, in contrast to the 15° case, is commensurate with the smaller unsteady forces measured for this case; the latter data are discussed in §4.

For the data in figure 16(*d*), there is a large separation between the reference probe and the measurement location (figure 1*b*). Such spatial separation (or temporal separation between trigger and instants of data sampling) can result in smearing in the eduction (Zaman & Hussain 1984); also, the further the departure from periodicity in the flow the larger is this smearing effect from probe separation. It was felt necessary to check this effect, and the measurements were repeated at $x/c = 1.5$ with the reference probe located at the same x-position. These data are shown in figure 18(*a*). Except for the time shift due to different trigger instants, essentially the same $\langle \Omega_z \rangle$ distribution is educted. One has to conclude that the departure from periodicity was not large and the triggering criterion used was sufficient to preclude significant smearing. The same conclusion was reached for the 22.5° case, by repeating the measurements at $x/c = 2.5$ with the reference probe located at the same x-position. These data are shown in figure 18(*b*) and should be compared with those in figure 17(*d*).

3.2.3. *Further on the bluff-body-shedding case*

In both figures 18(*b*) and 17(*d*) the (absolute) peak negative levels are significantly higher than the peak positive levels. But these levels approach each other with increasing x, as shown by measurements at $x/c = 3.5$ (figure 18*c*). If such equality in the peak $\langle \Omega_z \rangle$ levels were taken as a criterion, the flow structure for the 22.5° case is found to be still evolving at $x/c = 2.5$, an 'asymptotic state' being reached by the distance of about $x/c = 3.5$. Eduction farther downstream was not attempted as the corner flow effects should become increasingly prominent.

Referring back to figure 4(*a*), one notes that $f_s = 36$ Hz for the 22.5° case is coincident with the flexural resonance frequency of the airfoil. This raised the question of whether the flow was 'excited' in this case. In order to assess this, the eduction was repeated at another Reynolds number ($R_c = 0.3 \times 10^5$). The shedding frequency, $f_s = 13.5$ Hz, was different from the flexural resonance, which remained the same, at 36 Hz. The corresponding data are shown in figure 19(*a*). On comparison with figure 18(*b*), one finds that essentially the same flow structure has been educted. This provides evidence that the educted structure for $\alpha = 22.5°$ at $R_c = 0.75 \times 10^5$, being compared with the low-frequency case, is natural and not enhanced due to excitation.

Further eductions were done with an NACA0012 airfoil ($c = 10.2$ cm) at $\alpha = 22.5°$

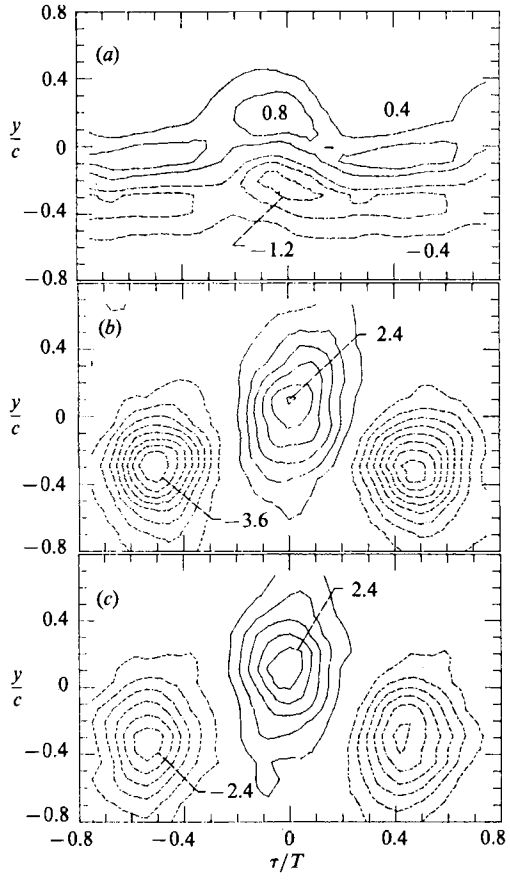

FIGURE 18. $\langle \Omega_z \rangle$ (c/U_∞) distribution: (*a*) at $x/c = 1.5$ for $\alpha = 15°$, (*b*) at $x/c = 2.5$ for $\alpha = 22.5°$, (*c*) at $x/c = 3.5$ for $\alpha = 22.5°$. Reference probe located at the measurement x-position in all cases.

and $R_c = 0.6 \times 10^5$, yielding $f_s = 50$ Hz. The data are shown in figure 19 (*b*, *c*) for the indicated x-stations. Comparing the similarity of these vorticity fields with the corresponding data in figure 17, one has to conclude that these distributions are quite robust and are also insensitive to the airfoil shape.

3.3. *Acoustic excitation and initial-condition effect*

Acoustic excitation at certain high frequencies was observed by Zaman *et al.* (1987) to completely eliminate the low-frequency oscillation. Referring back to figure 3, where excitation helped precipitate the oscillation, one notes a conflicting role of the excitation. This was explored systematically.

The wake oscillation amplitude u'_f, for the same α and probe location as in figure 3, was measured as a function of the acoustic excitation frequency f_p. A set of data is shown in figure 20 for $R_c = 0.75 \times 10^5$; the sound pressure level at the tunnel ceiling, L_R, was held constant at 104 dB. Consider the dashed curve for the flow without the screen. With excitation off ($f_p = 0$) there was only broadband energy at the low frequency, similar to that shown in figure 3 (*a*). Excitation in the f_p-range of about 2–6 kHz reduced this broadband energy. However, excitation at certain frequencies in the range 0.7–1.8 kHz precipitated the low-frequency (6 Hz) oscillation

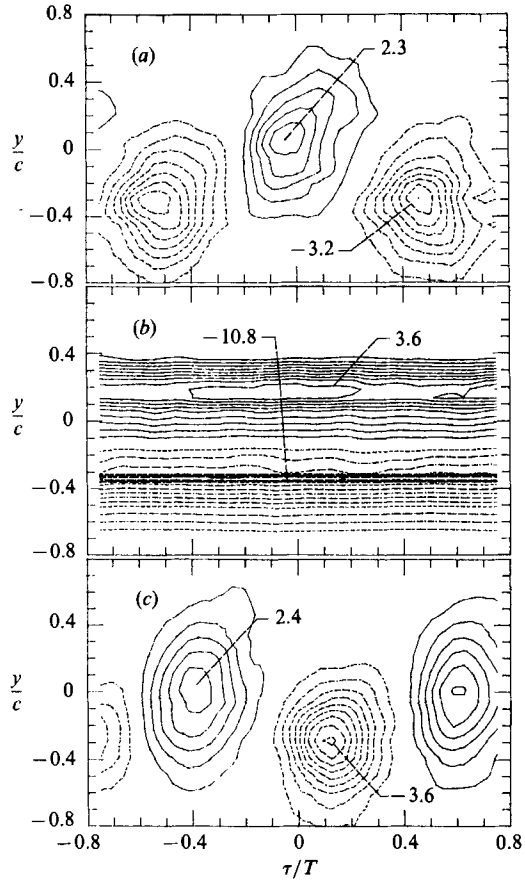

FIGURE 19. $\langle \Omega_z \rangle$ (c/U_∞) distributions: (*a*) at $x/c = 2.5$, $\alpha = 22.5°$, $R_c = 0.30 \times 10^5$; reference probe at the same x. (*b*) and (*c*) with NACA0012 airfoil ($c = 10.2$ cm) at $\alpha = 22.5°$ and $R_c = 0.6 \times 10^5$; reference probe as in figure 1(*b*). (*b*) $x/c = 0.5$, (*c*) $x/c = 2.5$.

as in figure 3(*b*). In contrast, the flow with the screen yielded the 6 Hz spectral spike naturally (as in figure 3*c*). Excitation in the lower f_p-range had an effect of slightly augmenting this spike. But in the higher f_p-range the excitation completely eliminated the 6 Hz spike. Only an effect similar to the latter was reported by Zaman *et al.* (1987).

Similar data for different R_c with airfoils of two different chords are shown in figure 21; the data from figure 20 are replotted for comparison. In each case, a similar effect of excitation can be noted as observed before. In a lower f_p-range, excitation enhances or generates the low-frequency oscillation, but suppresses it in a higher range of f_p.

3.3.1. *Separating-boundary-layer state*

The above data bear symptoms similar to those observed in free-shear-layer excitation studies. In particular, the high-f_p excitation effect appears very similar to the turbulence suppression phenomenon studied by Zaman & Hussain (1981*a*). In that work, high-frequency acoustic excitation was shown to eliminate unusually energetic coherent structures, through an early saturation of the imposed instability wave and the resulting early transition. The result was a remarkable suppression of

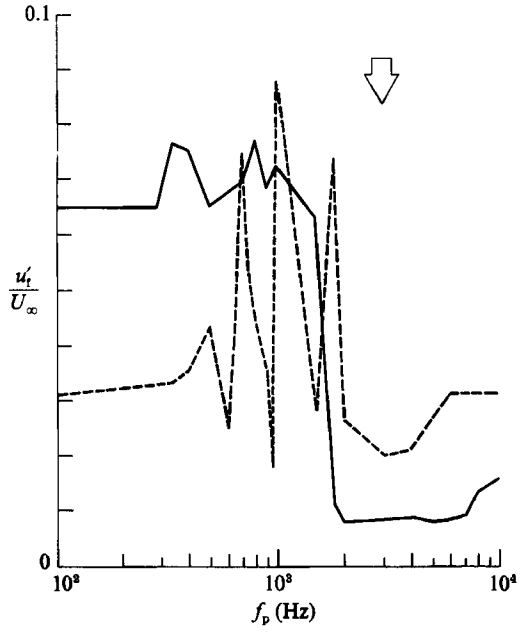

FIGURE 20. Variation of u'_t (at 5.75 Hz, $\delta f = 0.25$ Hz) with excitation frequency, measured at $x/c = 1.5$, $y/c = 0.15$ and $z = 0$; $R_c = 0.75 \times 10^5$. Solid line, $u'_\infty/U_\infty = 0.4\%$; dashed line, $u'_\infty/U_\infty = 0.1\%$. Arrow denotes 'natural instability frequency' of the separated shear layer.

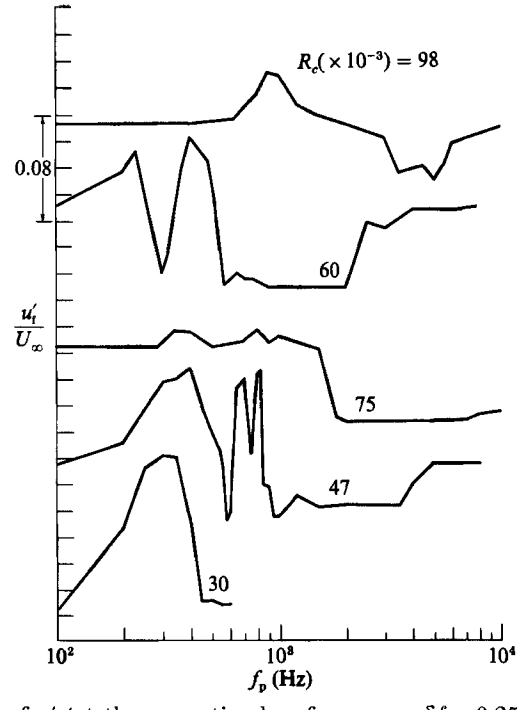

FIGURE 21. Variation of u'_t (at the respective low frequency, $\delta f = 0.25$ Hz) with f_p, measured at $x/c = 1.5$, $y/c = 0.15$ and $z = 0$. The lower three curves for the $c = 12.7$ cm airfoil, the upper two for the $c = 25.4$ cm (LRN) airfoil. $u'_\infty/U_\infty = 0.4\%$ in all cases.

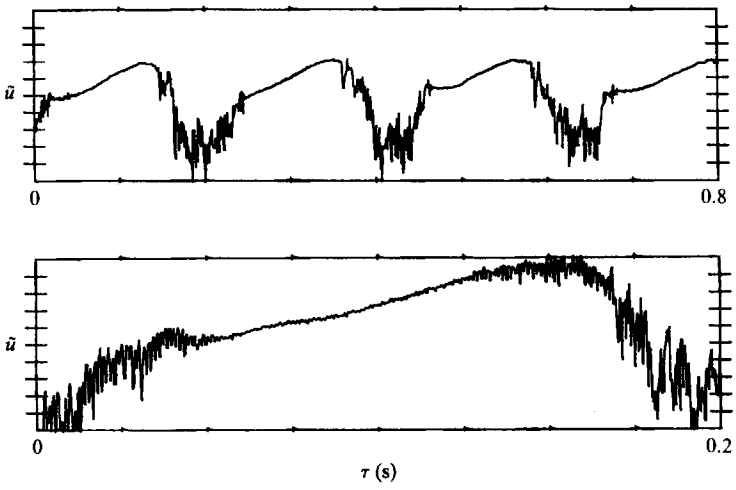

FIGURE 22. (Single) hot-wire output voltage at 6% chord location from the leading edge and about 1.5 mm from the surface. $\alpha = 15°$, $R_c = 0.47 \times 10^5$, $f_p = 800$ Hz, $L_R = 104$ dB, $u'_\infty/U_\infty = 0.4\%$. Arbitrary vertical scale (lower trace shown with expanded abscissa scale).

the fluctuation intensities observed downstream. The optimum effect occurred at an f_p about 40% higher than the natural 'initial roll-up' frequency. (The corresponding excitation Strouhal number, based on the initial momentum thickness, was 0.017.) The effect was found to diminish as a fully turbulent state of the initial boundary layer was approached (see also Zaman 1985). With the latter boundary-layer state, the fluctuation intensities were already low, and it was as if the excitation at Strouhal number 0.017 was 'tripping' the initial shear layer to full turbulence – an initial condition that yielded the lower fluctuation intensities downstream.

The f_p-range that eliminated the low-frequency oscillation is found to bear a relationship similar to the above with the 'initial roll-up' frequency of the separated shear layer, as discussed further shortly. Similarities can be observed, in the effect of the excitation, between the visualization pictures in figure 14 and those shown by Zaman & Hussain (1981*a*). This leads to the speculation that the low-frequency oscillation should not occur when the separating boundary layer is fully turbulent. On the other hand, the indications are that the phenomenon also does not occur with a laminar boundary layer. Thus, the increased free-stream turbulence or the trip or the lower-f_p excitation, needed for the phenomenon to take place, must have produced a certain transitional state of the separating boundary layer.

The characteristics of the speculated 'transitional state' remain unchartered. Measuring the fluctuating velocity profile near the separation point was contemplated but carrying it out with proper accuracy and resolution in the unsteady flow was considered formidable at this time. However, some observations on the separating-shear-layer instability were made. With a (single) hot wire placed near the uppermost reach of the fluctuating shear layer, time traces and spectra were obtained. Figure 22 shows such a time trace for $R_c = 0.47 \times 10^5$ with excitation at $f_p = 800$ Hz yielding a 4.5 Hz oscillation. The top trace clearly shows the periodicity at 4.5 Hz. The flow oscillation at 800 Hz can be barely observed in the relatively clean rising portion of the enlarged trace shown at the bottom. The corresponding u'-spectrum did show a small but clear peak at 800 Hz. This peak could be tracked up to about 15% chord location, with a broadband subharmonic peak emerging at about 9%

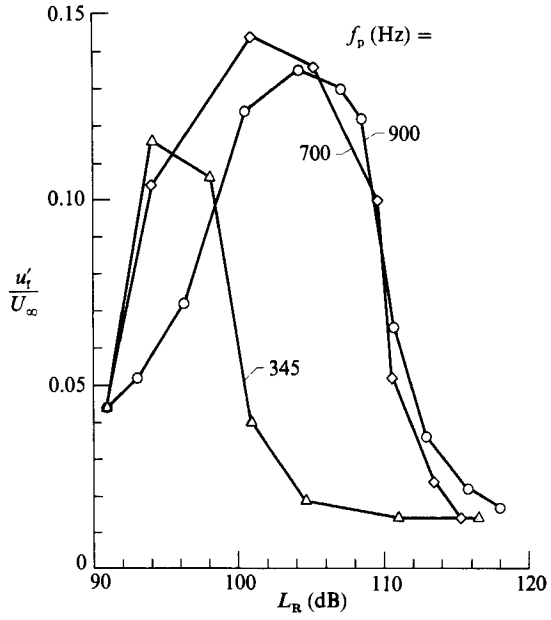

FIGURE 23. Excitation-amplitude effect on u'_f (at 4.5 Hz, $\delta f = 0.25$ Hz), measured at $x/c = 1.5$, $y/c = 0.15$ and $z = 0$. $\alpha = 15°$, $R_c = 0.47 \times 10^5$, $u'_\infty/U_\infty = 0.4\%$.

chord location. The spectral evolution resembled that observed in free shear layers (e.g. Kibens 1979), but the events were rendered complex due to the presence of the wall and especially the unsteadiness.

Single realizations of the spectra of signals as in figure 22, without any excitation, were examined. Occasionally, apparently when the cleaner part of the time trace was captured, the spectra exhibited a band of spikes roughly centred around a mean frequency, to be called f_m. f_m can be viewed as the natural, initial roll-up frequency of the separated shear layer, when the separation is the maximum. f_m, estimated from several realizations, is shown by the arrow in figure 20 for $R_c = 0.75 \times 10^5$. Thus, the enhancement of the low-frequency oscillation occurs when excitation is applied at f_p in the range 20%–60% of f_m. On the other hand, f_p ranging 100%–200% of f_m results in the suppression. The latter range covers the optimum f_p(about 140% of f_m) observed by Zaman & Hussain (1981*a*) in the free-shear-layer turbulence suppression phenomenon.

3.3.2. *Excitation-amplitude effect*

The excitation-amplitude effect in the generation of the low-frequency oscillation is documented in figure 23 for three different f_p. Obviously, the effect is pronounced in a range of amplitudes that depends on the frequency. In all cases, the low-frequency oscillation is suppressed at high amplitudes! (The microphone signal, at the highest amplitudes, was checked to be free of significant harmonic distortion.) Note that L_R is the SPL measured at a point on the ceiling above the airfoil and does not necessarily represent the level around the airfoil. But for a given f_p, increasing L_R should represent increasing excitation amplitude around the airfoil. 345 Hz is the fundamental cross-resonance of the test section. In this case, there is a fluctuating pressure node near the airfoil. The corresponding fluctuating (transverse) velocity intensity (v'_f) can be determined; for example, at $L_R = 100$ dB, v'_f would be about

4.8 mm/s. The amplitude-effect data remain little understood. Perhaps, the 'transitional state' speculated above depends on the amplitude. However, it is clear that the separating-boundary-layer state that gives rise to the low-frequency oscillation is very sensitive to the ambient condition.

3.4. *Further considerations*

3.4.1. *Reynolds-number and airfoil-shape effect*

Figure 24(*a*) shows the wake velocity spectra for various cases as indicated in the figure caption. For each case, the anticipated α-range was scanned to obtain optimum low-frequency oscillation in the wake. Traces (i)–(iii) are for the 12.7 cm chord (LRN) airfoil for which data have been discussed so far. These together with figure 3 show that the low-frequency oscillation takes place at $St_s \approx 0.02$ with this airfoil over the entire R_c range of 0.25×10^5–10^5. At the lowest R_c acoustic excitation was needed to produce the effect even with the screen in place. Traces (iv) and (v) are for the 25.4 cm chord (LRN) airfoil, with which the low-frequency oscillation took place at a higher α (= 17°) and St_s (= 0.033).

While the lower five curves in figure 24(*a*) are for airfoils that spanned the full width of the tunnel, data were also obtained with a shorter, 30.5 cm span (LRN) airfoil (c = 12.7 cm). It was mounted centrally in the 76 cm width of the tunnel. Trace (vi) represents this case showing that the oscillation occurred at about St_s = 0.025 at $\alpha = 18°$. This proved that the low-frequency oscillation was not due to an interaction between the corner flows from the junctions of the airfoil and the tunnel walls. In passing, let us note that the 'shedding frequency' of the junction vortices, from a cylinder and flat-plate junction, has been found by Thomas (1987) to be Reynolds-number dependent but approach the 'Strouhal frequency' at high R_e such as covered in the present experiment.

Two other airfoils were also tried: an NACA0012 (c = 10.2 cm) and a Wortmann FX 63-137 (c = 12.7 cm), both having span equal to the tunnel width. After considerable trial, the NACA0012 was found to produce similar fluctuations when tripping was applied near the leading edge on the under surface (as described earlier). Trace (vii) in figure 24(*a*) represents this case. The oscillation occurred at about $St_s = 0.022$ but could not be made as strong as in the other airfoil. With the Wortmann airfoil, which exhibits a different stall type, to be discussed shortly, all trials failed to produce the phenomenon.

Here, let us note that the LRN airfoil has a fairly sharp leading edge compared to the latter two. Surveys were also made by turning the latter two airfoils through 180° so that the sharp trailing edge took the place of the leading edge. This did not produce the phenomenon, which indicates that leading-edge sharpness is not a requisite in the generation of the phenomenon. The airfoil used by Farren (1935) also had a fairly rounded leading edge.

Additional wake velocity spectra are presented in figure 24(*b*) covering further parametric ranges. Traces (i)–(v) cover the entire R_c range of 0.15×10^5–3.0×10^5, available in the tunnel, over which the phenomenon consistently took place with the LRN airfoil. At this point we cannot be sure if the phenomenon will persist at even higher R_c. Within the range covered, however, there is no noticeable effect of R_c. Moss's (1979) observation of low-frequency force fluctuations covered the R_c-range up to 4×10^5 – which is still 'low' in airfoil aerodynamics terminology (Mueller 1985). However, McCullough & Gault (1951) had reported a 'violent buffetting' of an NACA 63_1-012 airfoil at $R_c = 5.8 \times 10^6$, akin to the observations of Farren (1935) and

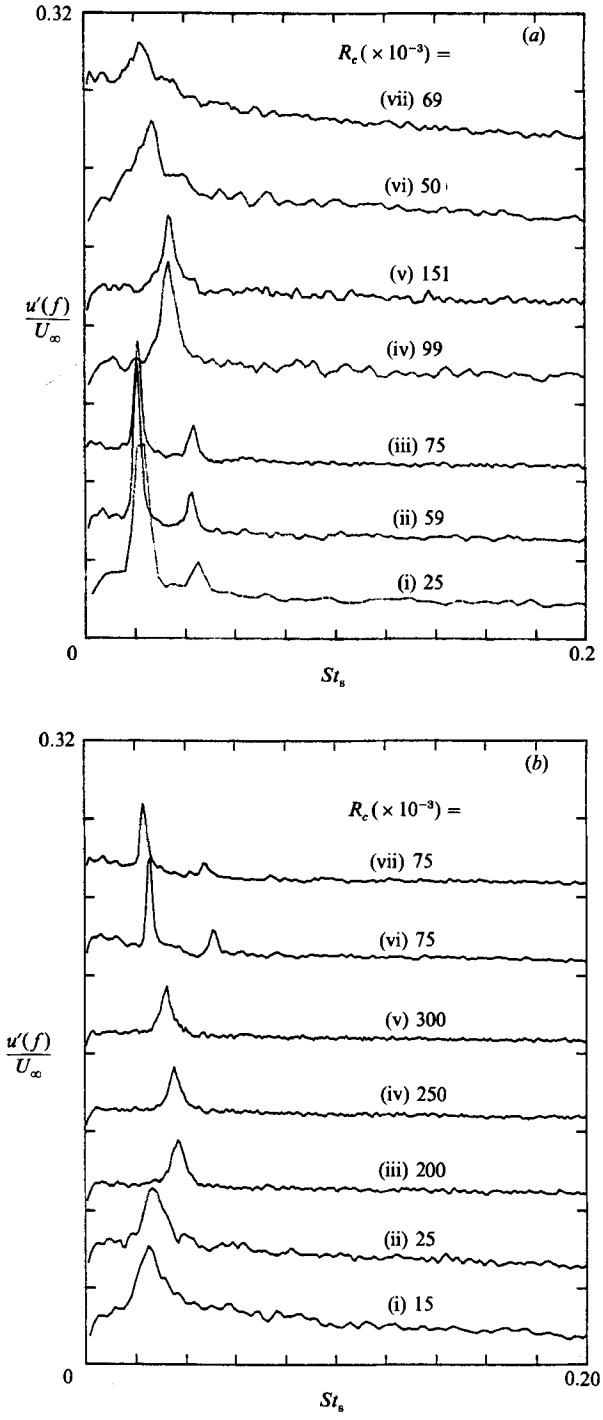

FIGURE 24. (*a*) u'-spectra at $x/c = 1.5$, $y/c = 0.15$ and $z = 0$, for different airfoils. (i)–(iii) for the $c = 12.7$ cm LRN airfoil at $\alpha = 15°$; (iv), (v) for $c = 25.4$ cm LRN airfoil at $\alpha = 17°$; (vi) for $c = 12.7$ cm LRN airfoil with 30 cm span, at $\alpha = 18°$; (vii) for $c = 10.2$ cm NACA0012 airfoil, $\alpha = 14°$. (*b*) u'-spectra as in (*a*) for LRN airfoils, but covering further parametric ranges. (i), (ii) $c = 7.3$ cm, $\alpha = 17°$; (iii)–(v) $c = 25.4$ cm, $\alpha = 16°$; (vi), (vii) $c = 12.7$ cm, $\alpha = 15°$, airfoil supported at 0.25*c* and 0.75*c* from leading edge, respectively.

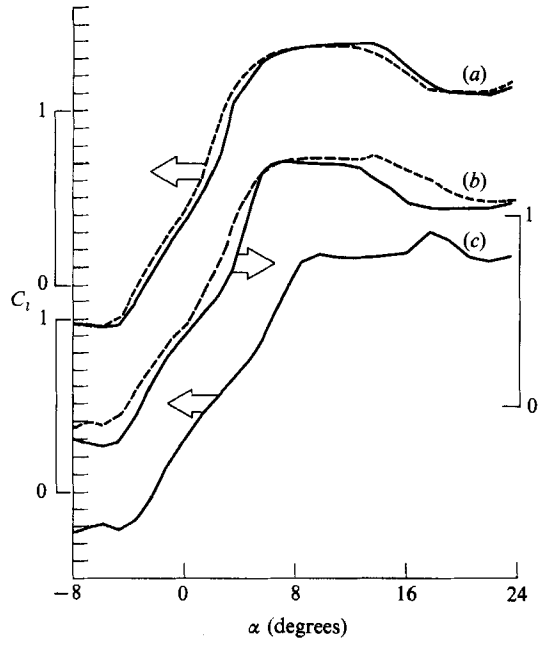

FIGURE 25. Lift coefficient *vs.* α for the LRN airfoil. (*a*) $c = 12.7$ cm, $R_c = 0.75 \times 10^5$, $u'_\infty/U_\infty = 0.4\,\%$. Solid curve for no excitation, dashed curve for $f_p = 3$ kHz. (*b*) $c = 12.7$ cm, $R_c = 0.75 \times 10^5$, $u'_\infty/U_\infty = 0.1\,\%$. Solid curve for no excitation, dashed curve for $f_p = 345$ Hz. (*c*) $c = 25.4$ cm, $R_c = 10^5$, $u'_\infty/U_\infty = 0.4\,\%$, no excitation.

Jones (1933). Unfortunately, this was not pursued any further. However, this is an indication that the phenomenon may not be typical of low Reynolds number only.

Traces (i) and (ii) in figure 24(*b*) were obtained with a smaller $c = 7.3$ cm chord airfoil. The St_s turned out to be about 0.025. Note that with the $c = 12.7$ cm and 25.4 cm airfoils St_s was found to be about 0.02 and 0.033, respectively. Thus, the data fail to reveal any consistent trend in the dependence of the value of St_s on the chord. For an airfoil of given chord, however, the value of St_s is found to remain approximately constant. The frequency scaling of the phenomenon remains unknown. Here, let us note that the 10.8 cm airfoil of Zaman *et al.* (1987) as well as the 15.2 cm airfoil of Farren (1935) both yielded an $St_s \approx 0.02$.

While the rest of the data in the paper were obtained with the airfoil supported at midchord, traces (vi) and (vii) in figure 24(*b*) represent data with the airfoil supported at two other chord locations. In spite of the small difference in St_s in (vii) it is clear that the phenomenon occurs in all support configurations. As the moment coefficient (C_m) distribution (*vs.* α) for different support configuration should be different, it is obvious that the phenomenon is not typical of any particular range of the C_m *vs.* α curve.

3.4.2. *Increase in the mean lift coefficient*

Five lift-coefficient, C_l, curves for the LRN airfoil are shown in figure 25. The two pairs on the top are for the $c = 12.7$ cm airfoil at $R_c = 0.75 \times 10^5$. The top pair (*a*) is for the flow with the screen. The solid line is for the flow without any excitation, producing the 6 Hz oscillation naturally at $\alpha = 15°$; the dashed line is with excitation

at 3 kHz completely eliminating the 6 Hz oscillation (see figure 20). Note that the lift coefficient is decreased as a result of the excitation around $\alpha = 15°$; a similar observation was made by Zaman *et al.* (1987). The pair in the middle (*b*) is without the screen. The solid curve is for the unexcited flow in which the low-frequency oscillation was absent. Comparing the two solid curves in these two pairs, one finds that just increasing the free-stream turbulence resulted in an increase in C_l throughout the α-range covered. A similar observation was made by Mangalam *et al.* (1986) for the same (LRN) airfoil by appropriate tripping on the upper surface.

The dashed curve in the second pair represents excitation at 345 Hz yielding the low-frequency oscillation. Note that there is an increase in C_l at all α, but more so around 15°. Thus, in both cases (*a*) and (*b*) the occurrence of the low-frequency oscillation is accompanied by an increase in the (mean) lift coefficient. In particular, a marked peak was observed for the 25.4 cm airfoil, as shown by the bottom curve (*c*) in figure 25, at around $\alpha = 17°$ where the low-frequency oscillation took place. The cause of the higher (mean) C_l is not clearly understood. The flow oscillations may be responsible for this. The energetic flow oscillations (at the low frequency) may result in a tendency towards reduced (overall) separation, causing the higher lift, just as excitation does in some cases, e.g. during post-stall conditions (Zaman *et al.* 1987). We note that Farren (1935) had also observed 'unusual peaks' in the lift curves – but only during 'pitch-up' motion of an oscillating airfoil.

3.4.3. *Influence of 'stall type'*

The most conspicuous difference of the Wortmann airfoil, which did not produce the low-frequency oscillation, is in its stall characteristics. With the same conditions as in figure 25, it exhibited a discontinuous lift at stall accompanied by significant hysteresis. At $R_c = 0.75 \times 10^5$, it stalled at about 14° when α was being increased but returned to the unstalled state at about 8° when α was being decreased (Zaman & McKinzie 1989).

From systematic observations of the separated flow, with nothing more than a Pitot tube and tuft technique, Jones (1933) made a lasting contribution to the field of airfoil aerodynamics. He described three types of stalling process associated with different airfoils. (1) With increasing α, separation occurred first near the trailing edge and then approached the leading edge. Found with airfoils 'R.A.F. 32' and 'Clark YH', the stall did not involve noticeable hysteresis. (Prior to the stall, a short separation bubble occurred with the former but not with the latter airfoil.) (2) With increasing α, a short bubble near the leading edge elongated and was followed by separation from the leading edge. No hysteresis was observed with the 'R.A.F. 28' and 'R.A.F. 30' airfoils exhibiting this type of stall. (3) Abrupt leading-edge separation took place with discontinuity in the lift curve accompanied by hysteresis. The model 'E' ('Airscrew') airfoil exhibited this type of stall. The three types of stall were further investigated by McCullough & Gault (1951), the type (2) stall having been referred to as the 'thin-airfoil stall'. It was noted that the stall exhibited by a given airfoil may not exactly fit one of the three types and may also depend upon R_c and ambient conditions.

In his study, Jones (1933, 1934) observed that 'violent force fluctuations' occurred with the first two stall types but not as prominently with the third. One of the distinctions between the first two types of stall was in the relative location of the large fluctuations on the lift curve – occurring at the incidence of maximum lift with type (2) but a few degrees above the incidence of maximum lift in type (1).

From the flow visualization pictures with varying α shown by Zaman *et al.* (1987),

and from inspection of the lift curves in figure 25, the LRN airfoil appears to be a borderline case between type (1) and type (2) stalls. The Wortmann airfoil, on the other hand, clearly fits the description of type (3) stall. The absence of the low-frequency oscillation in conjunction with appearance of stall hysteresis with the Wortmann airfoil closely matches Jones' observation for airfoil 'E'. In a way, the periodic switching between stall and unstall being studied here appears morphologically similar to the stall hysteresis phenomenon. Depending on the airfoil shape, it is as if the hysteresis effect replaces the low-frequency oscillation phenomenon. Jones (1933) had also commented, '... a study of the whole available data, including the pressure diagrams at the critical incidences, leads irresistibly to the conclusion that the flow changes which were responsible for the fluctuations were of the same kind as those which caused the discontinuity with aerofoil E..., except that, with E, either regime could be maintained for a long period and the details could be easily examined'.

3.4.4. *Stall flutter*

Bluff-body shedding has been shown to produce negligible flow fluctuations around the airfoil in the present study. In comparison, the low-frequency oscillation produces much larger fluctuations (see figures 5, 16–19). The fluctuations induced on the lift were measured for the two cases of §3.2. The fluctuation in C_l for the $\alpha = 15°$ case, to be further discussed in the next section, was found to be about 50% of the mean C_l. In comparison, the fluctuation for the 22.5° case was very small and estimated (from the lift-signal spectrum) to be only about 1% of the mean C_l.

Thus, the low-frequency oscillation could be a more effective mechanism in instigating stall flutter. Flutter of wings and blades is the self-sustained vibration occurring at the fundamental flexural or torsional resonances or at any or combination of their harmonics (Armstrong & Stevenson 1960). In turbomachinery bladings, flutter has been observed to be predominantly torsional (Halfman, Johnson & Haley 1951; Baker 1955). Avoiding flutter is a serious design consideration in turbomachinery as well as in propellers and wings. 'Stall flutter' denotes the condition when the flow is stalled during all or part of the oscillation cycle, in contrast to 'classical flutter' which takes place at lower incidences when the flow is attached.

Although flutter is the vibration at the structural resonant frequencies, the unsteady flow must be responsible for its sustenance. Without stimulation from the flow, the vibration would normally be expected to damp out. The aerodynamic aspect of flutter, of course, is the concern here. For a given blade or wing configuration, there exists a (critical) lower limit of free-stream speed (or the equivalent of it) – referred to in the literature as the 'flutter speed' – below which flutter does not occur. 'Flutter speed' has been often non-dimensionalized by the frequency and the chord and thus is inversely proportional to St_s for a given incidence. The lower limit in 'flutter speed' thus denotes an upper limit of St_s above which flutter is not expected to occur. If bluff-body shedding (and harmonics) were the primary stimulant to induce flutter, one would expect this upper limit of St_s to be greater than 0.2 and possibly most flutter frequency data to correspond to $St_s \approx 0.2$. However, a review of the literature clearly suggests that this upper limit is much lower than 0.2.

As mentioned in §1, this limit found by Armstrong & Stevenson (1960) was about 0.012 for flexural and about 0.05 for torsional flutter. Baker (1955) provided systematic data on torsional 'flutter speed' as a function of incidence while varying

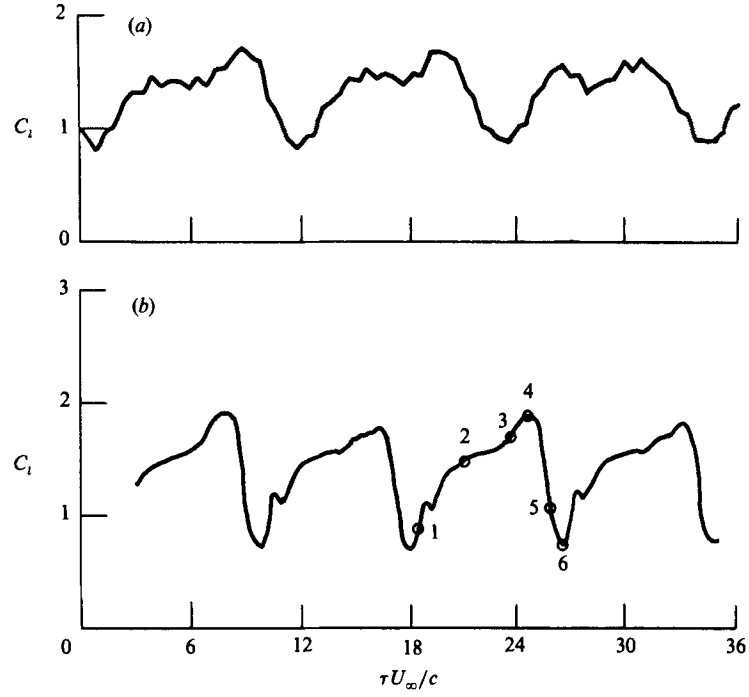

FIGURE 26. Lift-coefficient variation with time for the LRN airfoil at $\alpha = 15°$ and $R_c = 0.75 \times 10^6$. (*a*) Experiment, (*b*) computation.

stiffness, taper, twist, aspect ratio and various other parameters. The minimum 'flutter speed' occurring around 20° incidence, was independent of many of these parameters, and corresponded to an upper St_s limit of about 0.1. The flutter boundary data, for an NACA 64-012 airfoil, obtained in connection with space-shuttle wing design, cited by Ericsson (1986), also converts to an St_s range of 0.03–0.14. Thus, the *upper limit* of St_s in flutter has always been found to be significantly lower than the value 0.2, flutter usually having been observed at much lower values.

The above suggests that bluff-body or Kármán vortex shedding cannot be the flow mechanism by which flutter is initiated and sustained. The low-frequency oscillation under study – involving the periodic stalling and unstalling – is a much likelier description of the fluid dynamics of stall flutter. The force fluctuation measurements of Farren (1935), Jones (1933), Moss (1979) and the present study clearly support this notion.

4. Computational study of the flow

4.1. *Procedures*

An upwind-biased, implicit, approximate factorization, computer algorithm which solves the thin-layer approximation to the two-dimensional Navier–Stokes equations is used in the present analysis (Rumsey *et al.* 1986; Rumsey 1987). The algorithm is first-order accurate in time and second-order accurate in space. A quasi-one-dimensional characteristic analysis is used to explicitly determine the far-field boundary conditions. On the body, no-slip, adiabatic conditions along with a zero

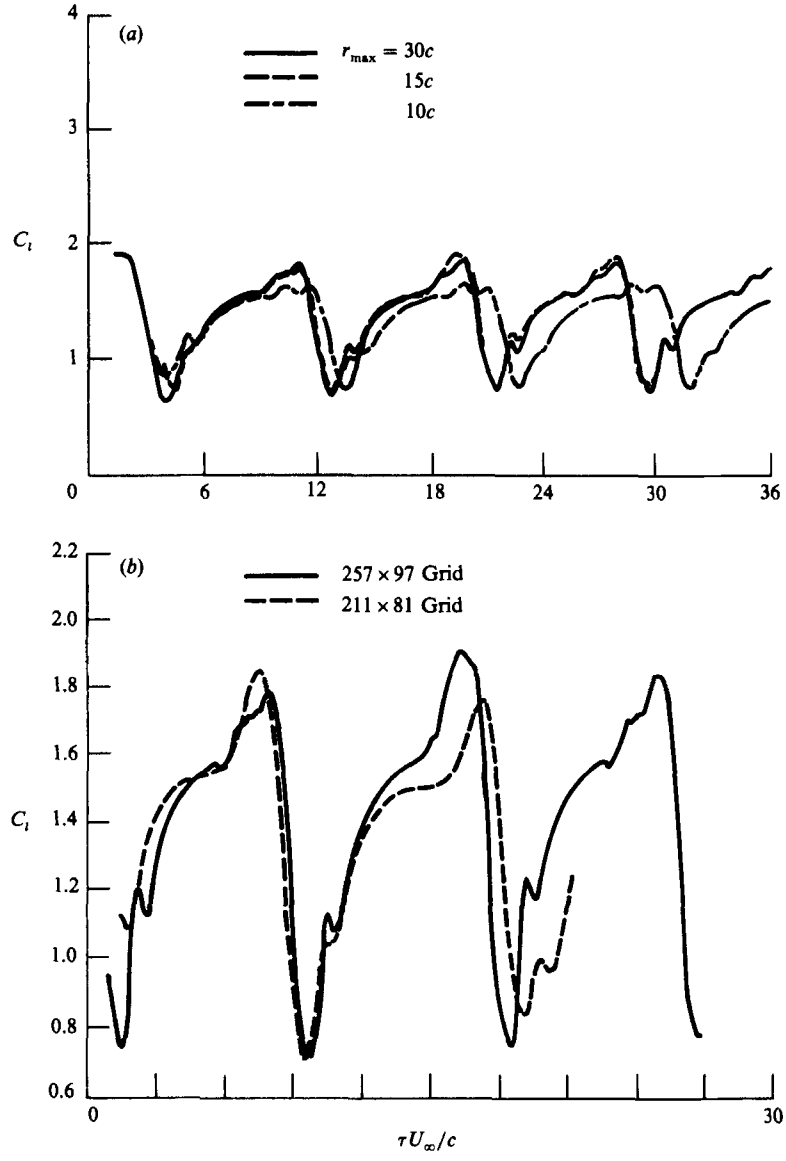

FIGURE 27. C_l variation with time: (*a*) with different computational domain boundaries. r_{max} is an average distance of the boundary from the airfoil. (*b*) With different grid density.

normal pressure gradient are applied. Although its applicability in unsteady stalled flow is questionable, the Baldwin–Lomax algebraic turbulence model is employed with transition location assumed to be at the leading edge.

The grid used is a 257×97 C-mesh with 176 points on the airfoil, having an outer boundary extent of 15c from the airfoil and a minimum average normal spacing at the wall of $0.0001c$. The latter spacing ensured about three grid points within the sublayer in the case under consideration. The computations were performed at a Mach number of 0.3. All computations were started from free-stream conditions, without any imposed perturbation, and were carried on until a quasi-periodic limit cycle was reached.

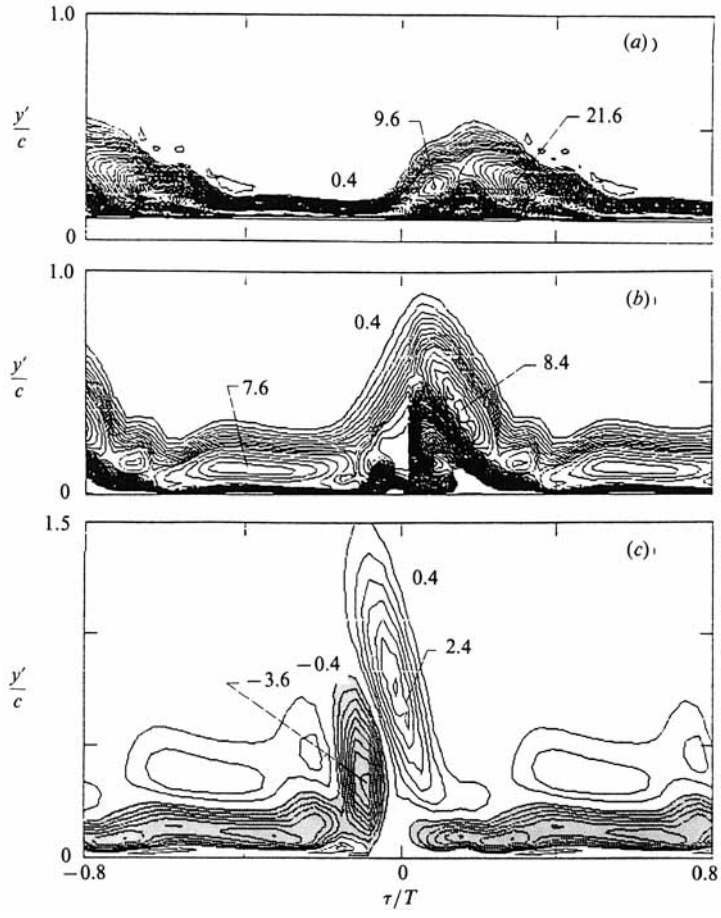

FIGURE 28. $\Omega_z(c/U_\infty)$ contours as in figure 16 but obtained computationally. y' is perpendicular distance from the chord line. Measurements at: (*a*) $x/c = 0$, (*b*) $x/c = 0.5$ and (*c*) $x/c = 1.5$.

4.2. *Computational results*

The computation was performed for the same airfoil shape (LRN), R_c ($= 0.75 \times 10^5$) and α ($= 15°$) as in the experiment. This yielded a low-frequency oscillation at $St_s = 0.03$. Corresponding lift-coefficient variation with time is shown in figure 26, compared with the experimentally measured variation. In spite of the difference in the period, the waveform shapes are observed to be quite similar. These data provided confidence that the computation was capturing the essence of the flow physics. The flow-field characteristics were then computed, in such detail as would be impossible to obtain experimentally.

A few critical questions are addressed first. Townsend, Rudy & Sirovich (1987) had encountered a low-frequency oscillation, in (laminar) Navier–Stokes computation of a cylinder wake, due to reflection from the computational domain boundary. A standing (acoustic) wave was set up giving rise to a low-frequency modulation of the Kármán vortex shedding, resulting in wake velocity spectra that had curious similarities to the experimental observation of Sreenivasan (1985). Townsend *et al.* (1987) traced the origin of the low-frequency modulation to half-wave acoustic resonance between the cylinder and the computational domain boundary. They

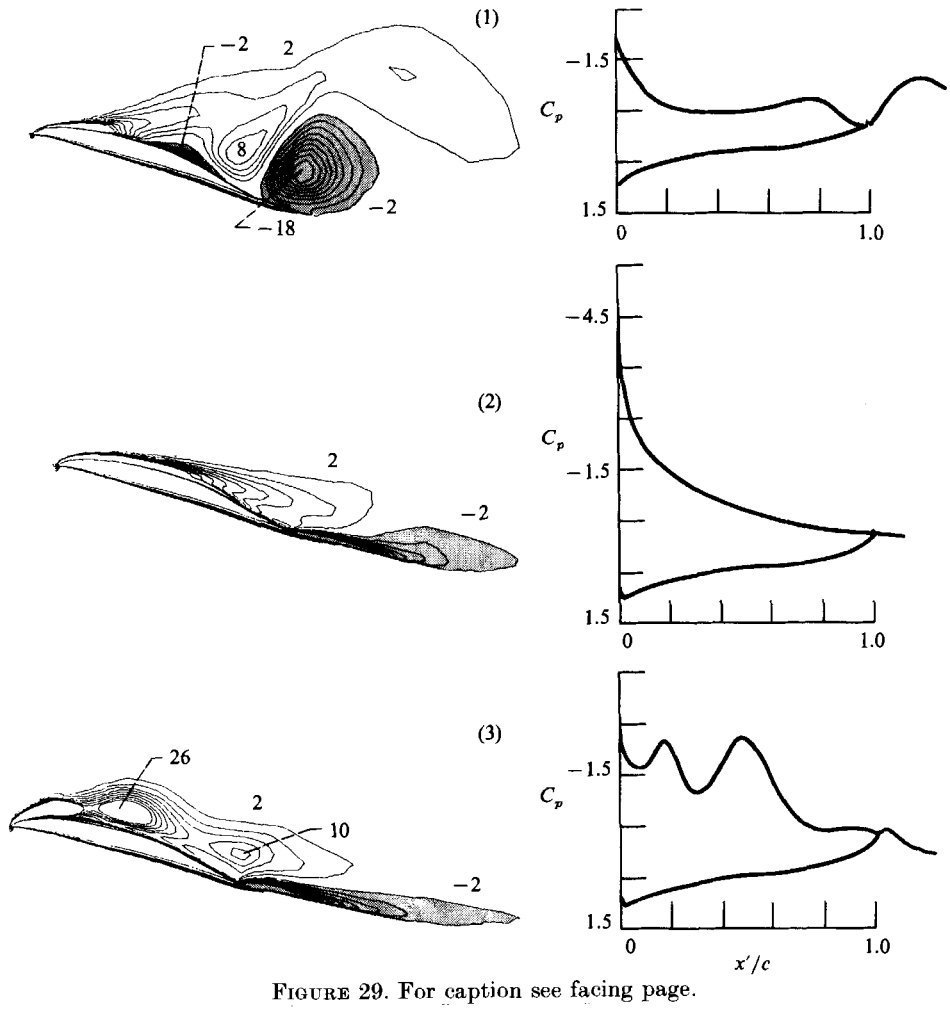

FIGURE 29. For caption see facing page.

showed it by simply extending the boundary, causing a commensurate decrease in the frequency.

Appropriate (non-reflective) boundary conditions were used in the present computation. However, possible residual reflection giving rise to standing waves was further probed by computation with shortened (10 c) and extended (30 c) C-mesh domains having 253×95 and 267×104 grid points, repectively. The results are shown in figure 27 (a) and it is clear that for grid extents larger than 15 c, variation in the boundary does not change the frequency or waveform of the C_l-variation. This disproves the existence of standing waves similar to those observed by Townsend *et al.* (1987), and establishes the adequacy of the 15 c extent of the computational domain.

In order to assess the effect of grid density on the unsteady solution, a coarser 211×81 grid was also employed. The resulting lift-coefficient history is compared with that from the finer grid in figure 27 (b). Results are very similar, with only slight differences in the global characteristics of the flow field.

The temporal distributions of Ω_z for three x-locations are shown in figure 28. These

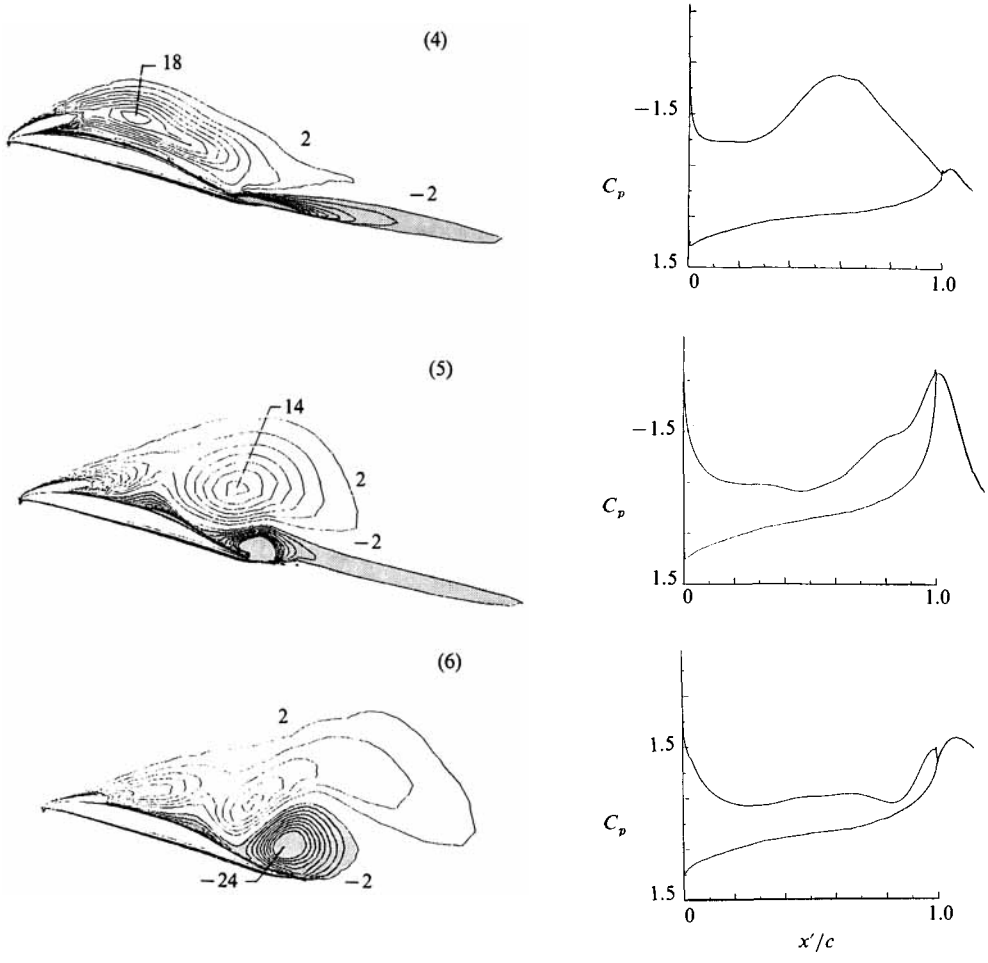

FIGURE 29. Spatial distributions of $\Omega_z(c/U_\infty)$ obtained computationally for the six phases marked on figure 26(*b*). Contour levels are at increments of 2. Corresponding C_p-distributions are shown on the right for each phase; x' is distance from leading edge.

data are constructed from spatial distributions computed for contiguous time steps. (Note that the bracket in Ω_z is omitted as these data are for a 'single realization' and are not ensemble averages.) The distributions in figures 28(*a*), 28(*b*) and 28(*c*) should be compared with those in figures 16(*a*), 16(*c*) and 16(*d*), respectively. One finds that the peak levels obtained computationally are somewhat higher. However, the overall distributions are similar to those found experimentally. The high levels diminish rapidly by the distance $x/c = 1.5$, and no significant 'roll-up' is observed.

The computed spatial distributions of Ω_z, at the phases marked 1–6 in figure 26 (*b*), are shown in figure 29. Also shown are the corresponding pressure coefficient (C_p)-distributions. In contrast to the data in figure 28, significant concentration of the vorticity is observed instantaneously. However, the flow structure changes rapidly, and drastically, e.g. between phases 1 and 2. Note that the distribution in figure 28 is constructed from the distribution of figure 29 at many time steps; but in the fast-evolving field, the temporal distribution appears quite different from the spatial distributions. Note also that in the computation it was easier to obtain the spatial

distributions, and difficult and time consuming to construct the temporal distributions. The reverse was the case in the experiment; it was possible to obtain the ensemble-averaged temporal distributions (figure 16), but to obtain the corresponding spatial distributions would be a formidable task.

Concerning the significance of the temporal and spatial distributions, either can be meaningful and important to the understanding of the flow physics. The spatial distributions, however, have the added advantage of corresponding more directly to the flow visualization pictures representing the flow field at certain instants (Zaman & Hussain 1981*b*). Referring back to figure 14, some similarities can be observed between the picture for the unexcited case with phase (5) in figure 29.

A concentration of counterclockwise vorticity is observed to form near the trailing edge in phase (5) of figure 29. The lift coefficient at this instant is approaching the minimum (figure 26). The vortex stays almost stationary and grows through phases (6) to (1), but then abruptly gets squashed in phase (2) when the lift has jumped to a high value. On the other hand, a concentration of clockwise vorticity first appearing at midchord in phase (3), having the appearance of a 'dynamic stall vortex' (McCroskey, Carr & McAlister 1975), grows to a maximum in phase (5). It moves slightly downstream during phases (3)–(5) but rapidly dissipates in phase (6) with the appearance of the counterclockwise vorticity. Note that about one chord downstream of the trailing edge, very little vorticity concentration occurs, commensurate with the distributions in figures 28(*c*) and 16(*d*).

The rapid changes in the C_p-distributions (figure 29) produce fluctuations in the lift coefficient as shown in figure 26(*b*). The 'sloshing' of the C_p-distribution on the upper surface also indicates large fluctuations in the moment coefficient. The moment coefficient, computed at about one-quarter chord, varied between -0.07 and -0.49, corresponding to the data in figure 29.

In the final stages of this investigation, a similar computation was also performed with a Wortmann airfoil at $R_c = 75000$ and $\alpha = 15°$. Recall that the low-frequency oscillation was not observed with this airfoil in the experiment. The computational results were also free of the low-frequency oscillations!

5. Conclusions

The present paper documents data on a phenomenon of low-frequency oscillation of flow over an airfoil that is different in many ways from the relatively well-known Kármán or bluff-body vortex shedding. Various questions have remained unanswered but the following inferences have been clearly made: (1) The phenomenon is hydrodynamic in nature and not due to a standing acoustic wave. (2) It is not a result of stimulation from structural resonances or blower instabilities. (3) The origin of the phenomenon traces to the upper surface of the airfoil near the leading edge, to a periodic switching between stalled and unstalled states. Over the airfoil the unsteady flow field is apparently two-dimensional. (4) The flow fluctuations are intense over the airfoil but decay rapidly downstream. The fluctuations impart unsteady forces to the airfoil much larger than that experienced during bluff-body shedding. The large unsteady forces must be given due consideration in various design codes. (5) The wake does not involve a Kármán vortex street. The intense spanwise vorticity shed from the upper surface is observed to disappear rapidly. (6) The unsteady flow field for the bluff-body shedding case has been shown to be insensitive to airfoil shape and Reynolds number within the range covered. The corresponding flow fluctuations have been found to be very small around the airfoil.

The Kármán vortex street 'rolls-up' within one half-chord and reaches an 'asymptotic state' by about three chords from the trailing edge.

Based on the results, the following conjectures are also made: (1) The phenomenon appears different from bluff-body shedding as well as other examples of self-sustained fluid mechanical oscillation such as edgetone, flow over cavities, supersonic jet screech, etc. In all the other examples there is always an obvious, imposed lengthscale that determines the wavelength of the oscillation. Usually, an integral multiple of the wavelength equals to the imposed lengthscale. In the present case, the tendency towards a constant Strouhal number indicates that the chord enters as a lengthscale; however, this lengthscale is equal to only a small fraction of the corresponding wavelength. (2) It takes place with airfoils exhibiting either the 'trailing-edge' or 'thin-airfoil' type stalls but does not with the 'leading-edge' type stall involving hysteresis. (3) Although observed at low Reynolds numbers, data from the literature suggest that it may persist at higher Reynolds number. (4) Stall flutter is not induced by bluff-body shedding. The unsteady flow field in stall flutter may be represented by that documented here for the low-frequency oscillation. (5) The phenomenon depends on the separating-boundary-layer state. It takes place with a 'transitional state' but not with laminar or fully turbulent states. This is why it has been found to be illusive and sensitive to ambient conditions. (6) The computational method, as employed in the present study utilizing the Baldwin–Lomax turbulence model, appears to have captured the essence of this 'transitional state', producing essentially the same phenomenon.

K. B. M. Q. Z. and D. J. M. would like to express their gratitude to several colleagues in the Internal Fluid Mechanics Division for providing encouragement and help in various forms during the course of this work. Special thanks are due to Dr E. J. Rice for taking an active interest throughout the study. Thanks are also due to Dr S. M. Mangalam for providing the coordinates of the airfoils, and to Mr A. Bar-Sever and Dr V. Kibens for constructive suggestions during the work.

REFERENCES

Anderson, W. K., Thomas, J. L. & Rumsey, C. L. 1984 Application of thin layer Navier–Stokes equations near maximum lift. *AIAA Paper* 84-0049.

Armstrong, E. K. & Stevenson, M. A. 1960 Some practical aspects of compressor blade vibration. *J. R. Aero. Soc.* **64**, 117–130.

Baker, J. E. 1955 The effects of various parameters, including Mach number, on propeller blade flutter with emphasis on stall flutter. *NACA TN*-3357.

Brooks, T. F. & Schlinker, R. H. 1983 Progress in rotor broadband noise research. *Vertica* **7**, 287–307.

Carmichael, B. H. 1981 Low Reynolds number airfoil survey: vol. I. *NASA Contractor Rep.* 165803.

Cendenese, A., Cerri, G. & Ianetta, S. 1981 Experimental analysis of the wake behind an isolated cambered airfoil. *Proc. IUTAM Symp. Unsteady Turbulent Shear Flows*, pp. 272–284. Springer.

Ericsson, L. E. 1986 Effect of Karman vortex shedding on airfoil flutter. *AIAA Paper* 86-1789.

Farren, W. S. 1935 The reaction on a wing whose angle of incidence is changing rapidly. Wind tunnel experiments with a short period recording balance. *Rep. & Mem.* 1648. Aeronautics Laboratory, Cambridge.

Halfman, R. L., Johnson, H. C. & Haley, S. M. 1951 Evaluation of high-angle-of-attack aerodynamic-derivative data and stall-flutter prediction techniques. *NACA TN*-2533

JONES, B. M. 1933 An experimental study of the stalling of wings. *Aero. Res. Counc. R & M* 1588. Aeronautics Laboratory, Cambridge.

JONES, B. M. 1934 Stalling. *J. R. Aeronaut. Soc.* **38**, 753–770.

KIBENS, V. 1979 Discrete noise spectrum generated by an acousically excited jet. *AIAA Paper* 79-0592.

MANGALAM, S. M., BAR-SEVER, A., ZAMAN, K. B. M. Q. & HARVEY, W. D. 1986 Transition and separation control on a low-Reynolds-number airfoil. *Proc. Intl Conf. on Aerodynamics at Low Reynolds Numbers, London.*

MCCROSKEY, W. J., CARR, L. W. & MCALISTER, K. W. 1975 Dynamic stall experiments on oscillating airfoils. *AIAA Paper* 75-125.

MCCULLOUGH, G. B. & GAULT, D. E. 1951 Examples of three representative types of airfoil-section stall at low speed. *NACA TN*-2502.

MOSS, N. J. 1979 Measurements of aerofoil unsteady stall properties with acoustic flow control. *J. Sound Vib.* **65**, 505–520.

MOTALLEBI, F. & NORBURY, J. F. 1981 The effect of base bleed on vortex shedding and base pressure in compressible flow. *J. Fluid Mech.* **110**, 273–292.

MUELLER, T. J. 1985 Low Reynolds number vehicles. *AGARD-AG*-288.

PARKER, R. 1966 Resonance effects in wake shedding from parallel plates: some experimental observations. *J. Sound Vib.* **4**, 62–72.

ROCKWELL, D. 1983 Oscillations of impinging shear layers. *AIAA J.* **21**, 645–664.

ROSHKO, A. 1954 On the drag and shedding frequency of two-dimensional bluff bodies. *NACA TN*-3169.

RUMSEY, C. L. 1987 A computational analysis of flow separation over five different airfoil geometries at high angles-of-attack. *AIAA Paper* 87-0188.

RUMSEY, C. L., THOMAS, J. L., WARREN, G. P. & LIU, G. C. 1986 Upwind Navier–Stokes solutions for separated periodic flows. *AIAA Paper* 86-0247.

SCHLICHTING, H. 1979 *Boundary Layer Theory.* McGraw-Hill.

SIMPSON, R. L. 1985 Two-dimensional turbulent separated flow. *AGARDograph* 287.

SREENIVASAN, K. R. 1985 Transitional and turbulent wakes and chaotic dynamical systems. In *Nonlinear Dynamics of Transcritical Flows*, pp. 59–80. Springer.

THOMAS, A. S. W. 1987 The unsteady characteristics of laminar juncture flow. *Phys. Fluids* **30**, 283–285.

TOWNSEND, J. C., RUDY, D. H. & SIROVICH, L. 1987 Computation and analysis of a cylinder wake flow. Presented at the *ASME Fluids Engineering Spring Conference, Cincinnati, Ohio, June 15–17.*

VAN ATTA, C. W. & GHARIB, M. 1987 Ordered and chaotic vortex streets behind circular cylinders at low Reynolds numbers. *J. Fluid Mech.* **174**, 113–133.

VAN DYKE, M. 1982 *An Album of Fluid Motion.* Parabolic.

ZAMAN, K. B. M. Q. 1985 Far-field noise of a subsonic jet under controlled excitation. *J. Fluid Mech.* **152**, 83–111.

ZAMAN, K. B. M. Q., BAR-SEVER, A. & MANGALAM, S. M. 1987 Effect of acoustic excitation on the flow over a low-*Re* airfoil. *J. Fluid Mech.* **182**, 127–148.

ZAMAN, K. B. M. Q. & HUSSAIN, A. K. M. F. 1981*a* Turbulence suppression in free shear flows by controlled excitation, *J. Fluid Mech.* **103**, 133–159.

ZAMAN, K. B. M. Q. & HUSSAIN, A. K. M. F. 1981*b* Taylor hypothesis and large-scale coherent structures. *J. Fluid Mech.* **112**, 379–396.

ZAMAN, K. B. M. Q. & HUSSAIN, A. K. M. F. 1984 Natural large-scale structures in the axisymmetric mixing layer. *J. Fluid Mech.* **138**, 325–351.

ZAMAN, K. B. M. Q. & MCKINZIE, D. J. 1988 A natural low frequency oscillation in the wake of an airfoil near stalling conditions. *AIAA Paper* 88-0131.

ZAMAN, K. B. M. Q. & MCKINZIE, D. J. 1989 Control of 'laminar separation' over airfoils by acoustic excitation. *AIAA Paper* 89-0565.